Miner Deposita (2009) 44:611–646
DOI 10.1007/s00126-009-0239-1

ARTICLE

Late Cretaceous porphyry Cu and epithermal Cu–Au association in the Southern Panagyurishte District, Bulgaria: the paired Vlaykov Vruh and Elshitsa deposits

Kalin Kouzmanov · Robert Moritz · Albrecht von Quadt · Massimo Chiaradia · Irena Peytcheva · Denis Fontignie · Claire Ramboz · Kamen Bogdanov

Received: 18 December 2008 / Accepted: 13 March 2009 / Published online: 10 April 2009

Abstract Vlaykov Vruh–Elshitsa represents the best example of paired porphyry Cu and epithermal Cu–Au deposits within the Late Cretaceous Apuseni–Banat–Timok–Srednogorie magmatic and metallogenic belt of Eastern Europe. The two deposits are part of the NW trending Panagyurishte magmato-tectonic corridor of central Bulgaria. The deposits were formed along the SW flank of the Elshitsa volcano-intrusive complex and are spatially associated with N110-120-trending hypabyssal and subvolcanic bodies of granodioritic composition. At Elshitsa, more than ten lenticular to columnar massive ore bodies are discordant with respect to the host rock and are structurally controlled. A particular feature of the mineralization is the overprinting of an early stage high-sulfidation mineral assemblage (pyrite ± enargite ± covellite ± goldfieldite) by an intermediate-sulfidation paragenesis with a characteristic Cu–Bi–Te–Pb–Zn signature forming the main economic parts of the ore bodies. The two stages of mineralization produced two compositionally different types of ores—massive pyrite and copper–pyrite bodies. Vlaykov Vruh shares features with typical porphyry Cu systems. Their common geological and structural setting, ore-forming processes, and paragenesis, as well as the observed alteration and geochemical lateral and vertical zonation, allow us to interpret the Elshitsa and Vlaykov Vruh deposits as the deep part of a high-sulfidation epithermal system and its spatially and genetically related porphyry Cu counterpart, respectively. The magmatic–hydrothermal system at Vlaykov Vruh–Elshitsa produced much smaller deposits than similar complexes in the northern part of the Panagyurishte district (Chelopech, Elatsite, Assarel). Magma chemistry and isotopic signature are some of the main differences between the northern and southern parts of the district. Major and trace element geochemistry of the Elshitsa magmatic complex are indicative for the medium- to high-K calc-alkaline character of the magmas. $^{87}Sr/^{86}Sr_{(i)}$ ratios of igneous rocks in the range of 0.70464 to 0.70612 and $^{143}Nd/^{144}Nd_{(i)}$ ratios in the range of 0.51241 to 0.51255 indicate mixed crustal–mantle

Editorial handling: R. Romer

K. Kouzmanov (✉) · R. Moritz · M. Chiaradia · D. Fontignie
Section des Sciences de la Terre, Université de Genève,
Rue des Maraîchers 13,
1205 Genève, Switzerland
e-mail: kalin.kouzmanov@unige.ch

K. Kouzmanov · C. Ramboz
Institut des Sciences de la Terre d'Orléans (ISTO-CNRS),
1A, rue de la Férollerie,
45071 Orléans Cedex 2, France

A. von Quadt · I. Peytcheva
Institute of Isotope Geochemistry and Mineral Resources,
ETH Zentrum,
Clausiusstrasse 25,
8092 Zurich, Switzerland

I. Peytcheva
Central Laboratory of Mineralogy and Crystallography,
BAS,
1113 Sofia, Bulgaria

K. Bogdanov
Sofia University "St. Kliment Ohridski",
15 Tsar Osvoboditel Bd.,
1000 Sofia, Bulgaria

components of the magmas dominated by mantellic signatures. The epsilon Hf composition of magmatic zircons (+6.2 to +9.6) also suggests mixed mantellic–crustal sources of the magmas. However, Pb isotopic signatures of whole rocks ($^{206}Pb/^{204}Pb$=18.13–18.64, $^{207}Pb/^{204}Pb$=15.58–15.64, and $^{208}Pb/^{204}Pb$=37.69–38.56) along with common inheritance component detected in magmatic zircons also imply assimilation processes of pre-Variscan and Variscan basement at various scales. U–Pb zircon and rutile dating allowed determination of the timing of porphyry ore formation at Vlaykov Vruh (85.6±0.9 Ma), which immediately followed the crystallization of the subvolcanic dacitic bodies at Elshitsa (86.11±0.23 Ma) and the Elshitsa granite (86.62±0.02 Ma). Strontium isotope analyses of hydrothermal sulfates and carbonates ($^{87}Sr/^{86}Sr$= 0.70581–0.70729) suggest large-scale interaction between mineralizing fluids and basement lithologies at Elshitsa–Vlaykov Vruh. Lead isotope compositions of hydrothermal sulfides ($^{206}Pb/^{204}Pb$=18.432–18.534, $^{207}Pb/^{204}Pb$=15.608–15.647, and $^{208}Pb/^{204}Pb$=37.497–38.630) allow attribution of ore-formation in the porphyry and epithermal deposits in the Southern Panagyurishte district to a single metallogenic event with a common source of metals.

Keywords Epithermal · Porphyry · Radiogenic isotopes · U–Pb dating · Panagyurishte district · Srednogorie · Bulgaria

Introduction

Spatial and genetic association between high-sulfidation epithermal precious metal and porphyry copper (±gold) deposits is a common feature of many mineral districts along active continental margins worldwide (e.g., Corbett and Leach 1998; Hedenquist et al. 1998; Muntean and Einaudi 2001; Sillitoe and Hedenquist 2003). Modern interpretations suggest various sources for the mineralizing fluids in the shallow epithermal environment of these systems—from dominantly magmatic to mixed magmatic–meteoric; a consensus exists concerning the prevailing magmatic origin of the fluids in the deeper porphyry environment (Arribas 1995; Sillitoe and Hedenquist 2003; Heinrich 2005; Seedorff et al. 2005). The transition between porphyry and epithermal environments, including evolution of the fluid composition and of the sulfidation state of the mineralizing fluids, lateral and vertical zonation in the distribution of wallrock alteration zones, and ore mineral assemblages has been noted in many Tertiary mineral districts, where tectonic and erosional processes did not significantly affect the original architecture of the magmatic–hydrothermal system (e.g., Cooke and Bloom 1990; Muntean and Einaudi 2000, 2001, Brathwaite et al. 2001; Müller et al. 2002), while Mesozoic and older systems are rarely well preserved (e.g. Kesler et al. 2005; Chambefort and Moritz 2006; Chambefort et al. 2007).

The Upper Cretaceous Apuseni–Banat–Timok–Srednogorie (ABTS) belt in Eastern Europe (Berza et al. 1998; Ciobanu et al. 2002; Heinrich and Neubauer 2002; Popov et al. 2002) is a metallogenic province enclosing important parts of the copper and gold reserves of the European continent and is the westernmost branch of the planetary-scale Tethyan Eurasian copper belt (Jankovic 1977). In Bulgaria, this belt coincides with a Late Cretaceous magmatic arc, hosting important porphyry Cu and epithermal Cu–Au deposits. Until the mid-1990s, the epithermal Cu–Au deposits in the intensively mineralized central part of this zone, known as the Panagyurishte mineral district (Bogdanov 1980), were described by most of the authors as "volcanic-hosted massive sulfides." Nowadays, they are recognized as typical examples of high-sulfidation epithermal systems (Mutafchiev and Petrunov 1996; Moritz et al. 2004).

In this contribution, we studied the magmatism and ore formation in the Elshitsa magmatic complex in the southern part of the Panagyurishte district, hosting the spatially associated Vlaykov Vruh porphyry Cu and the Elshitsa epithermal Cu–Au deposits, as well as several other small deposits and ore occurrences. Our investigation was focused on: (1) the petrological and geochemical characterization of the Elshitsa volcano-intrusive complex; (2) the mineral paragenesis at Vlaykov Vruh and Elshitsa; (3) radiogenic isotope tracing, and (4) high-precision U–Pb dating of magmatic and hydrothermal events. This approach allows us to provide new insights into the processes of magma generation that gave rise to magmatic–hydrothermal ore formation at the porphyry–epithermal interface, in one of the best examples of a tight porphyry–epithermal association within the Cretaceous ABTS belt in Eastern Europe.

Geological setting of the Panagyurishte district

The Panagyurishte ore district (Popov and Popov 1997, 2000; Popov et al. 2003) consists of a NNW-SSE trending alignment of porphyry and epithermal Cu–Au deposits situated 60 to 90 km east of Sofia (Fig. 1) in the central part of the Bulgarian segment of the ABTS belt known as the Srednogorie zone. The Srednogorie zone is an 80- to 100-km wide, east–west oriented tectono-magmatic unit situated between the Balkan zone to the north and the Rhodopean Massif to the south (Fig. 1a and b; Boccaletti et al. 1974; Aiello et al. 1977; Dabovski et al. 1991). The Central Srednogorie belongs to the undivided and rear part of the Late Cretaceous island arc system in Bulgaria (Fig. 1b; Dabovski et al. 1991; Kamenov et al. 2000).

The main characteristics of basement lithologies, Mesozoic sedimentary cover and Late-Cretaceous magmatism of

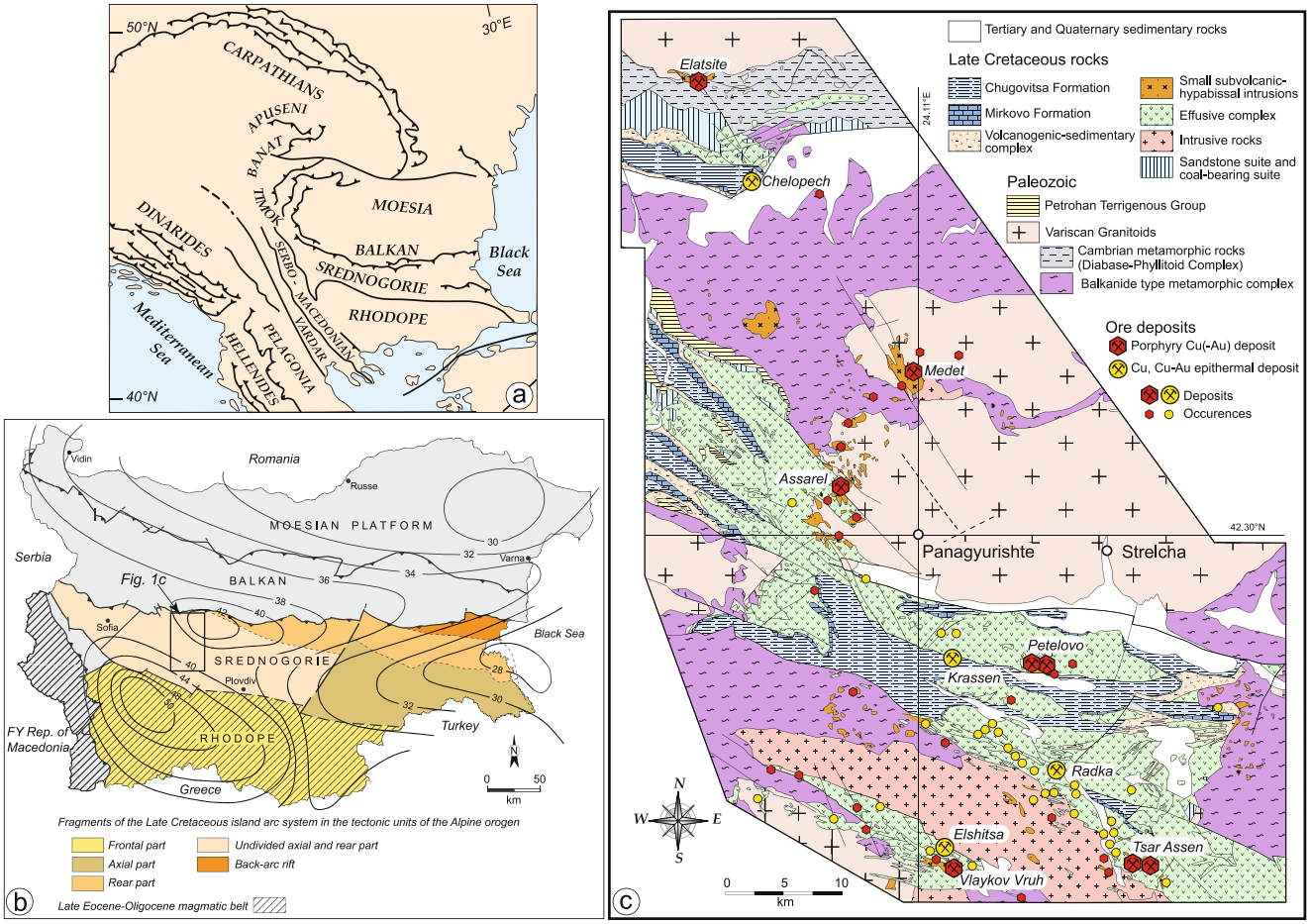

Fig. 1 **a** Position of the Srednogorie zone within its Alpine tectonic framework; **b** Tectonic units in Bulgaria. The Srednogorie zone is constituted of fragments of a Late Cretaceous island arc system. Crustal thickness in kilometers is indicated as well (modified after Yossifov and Pčelarov 1977; Dabovski et al. 1991; Kamenov et al. 2003a); **c** Simplified geological map of the Panagyurishte ore district (modified after Popov and Popov 2000). Location of major porphyry Cu–Au and epithermal Cu and Cu–Au deposits and occurrences are shown

the Panagyurishte district are summarized in Table 1. The Panagyurishte district presently constitutes a mosaic of horst and graben structures delimited by regional ~N110-120 trending transform faults, which resulted from trans-tensional, dextral strike-slip tectonics (Ivanov et al. 2001; Chambefort and Moritz 2006).

Porphyry copper mineralisation in the district is commonly centered on relatively small, approximately 1 km^2, subvolcanic bodies, which usually crosscut the volcanic edifices or are intruded into pre-Mesozoic basement (Strashimirov et al. 2002, 2003; Fig. 1c). Elatsite, Medet, and Assarel are the largest porphyry Cu–Au deposits and are located in the northern part of the district, whereas Tsar Assen and Vlaykov Vruh in the southern part are much smaller (Table 1; Fig. 1c). Drew (2005) recently interpreted the three largest porphyry copper deposits in Northern Panagyurishte as being formed in extensional fracture zones, along the edges of strike-slip fault duplex.

Based on current concepts on the genesis of magmatic–hydrothermal systems (e.g., Hedenquist and Lowenstern 1994; Hedenquist et al. 2000, 2001; Einaudi et al. 2003), the epithermal high-sulfidation Cu–Au deposits in the Panagyurishte district were interpreted as genetically linked to the porphyry Cu (–Au) systems, thus confirming the early interpretation of Dimitrov (1960) who first described these deposits as "epithermal to mesothermal epigenetic, usually structurally controlled, and formed by replacement and open-space deposition processes, with preferential development of alteration zones and ore bodies within the volcano-sedimentary units." The largest deposit of this type—Chelopech, is located in the Northern Panagyurishte, while the Southern Panagyurishte hosts only small or sub-economic ore deposits (Table 1).

Table 1 Geological setting and ore deposit types in the Panagyurishte district

Pre-Mesozoic basement	Mesozoic sedimentary cover	Late-Cretaceous magmatism		Ore deposits (from N to S)	Size of the deposits
- Paleozoic Balkanide type high-grade amphibolite facies metamorphic complex (Ivanov 1989a, b) or Srednogorie type metamorphic rocks (Cheshitev et al. 1995)	- Late Carboniferous to Jurassic clastic and carbonate sedimentary rocks - Petrohan Terrigenous Group – unconformably covering the basement lithologies;	- Andesites predominate in the northern and central parts of the district; dacitic volcanic rocks are more abundant in the southern sector, whereas rhyodacites and rhyolites occur exclusively in the central and southern parts (Dimitrov 1960; Ignatovski et al. 1990; Daieva and Chipchakova 1997; Lilov and Chipchakova 1999; Kouzmanov et al. 2001; Stoykov et al. 2004; Popov 2005; von Quadt et al. 2005; Kamenov et al. 2007). Due to a deeper erosional level, intrusive rocks become more abundant in the south (Ivanov et al., 2002).	Northern Panagyurishte district	Elatsite porphyry Cu-Au (-PGE) (in operation since 1981)	mined out 165 Mt @ 0.38 % Cu and 0.21 g/t Au; reserves 154 Mt @ 0.33 % Cu, 0.96 g/t Au, 0.19 g/t Ag, 0.007 g/t Pd and 0.002 g/t Pt (Strashimirov et al. 2002; Tarkian et al. 2003)
	- Sandstone suite – Turonian conglomerates and sandstones (Moev and Antonov 1978)	- Magmas are dominantly metaluminous and LILE-enriched with prevailing high-K calc-alkaline and shoshonitic trends (Daieva and Chipchakova 1997; Kamenov et al. 2007). The only exception is the Elshitsa magmatic structure in the southern part of the district which shows a typical calc-alkaline trend (Ignatovski et al. 1990; Kamenov et al. 2007). Geochemical signatures are typical of island-arc magmas in a subduction-related geodynamic setting (Boccaletti et al. 1974; Stanisheva-Vassileva 1980; von Quadt et al. 2005; Kamenov et al. 2007).		Chelopech HS epithermal Cu-Au (in operation since 1954)	total of past production and remaining resources 42.5 Mt @ 1.28 % Cu, 3.4 g/t Au and 8.4 g/t Ag (Moritz et al. 2004)
- Cambrian-Ordovician low-grade metamorphic Diabase-Phyllitoid Complex or Berkovitsa Group (Haydoutov 2001)	- Coniacian to Maastrichtian clastic terrigenous sequences with subordinate pelagic marls, shales, turbidites, and volcanic intercalations (Karagjuleva et al. 1974; Aiello et al. 1977; Nachev and Nachev 1986).			Medet porphyry Cu (1964-1993)	163 Mt @ 0.32 % Cu, 0.1 g/t Au (Strashimirov et al. 2002)
				Assarel porphyry Cu (in operation since 1976)	mined out 100 Mt @ 0.53% Cu ; reserves 254 Mt @ 0.41% Cu (Strashimirov et al. 2002)
- Variscan (300-350 Ma) gabbrodiorites, quartz-diorites, tonalites, and granodiorites-granites intruding the metamorphic rocks (Dabovski et al. 1972; Peytcheva and von Quadt 2004; Carrigan et al. 2005).		- Recent radiogenic (Pb, Sr, Nd, Hf) isotope data along with U-Pb geochronological studies (von Quadt et al. 2005 and references therein) reveal the mixed crustal-mantle source of the magmas, with a progressively increasing mantle component towards the Southern Panagyurishte district in parallel with the migration of a 14-m.y.-long protracted magmatic and ore-forming activity, starting at ca. 92 Ma in the north at Elatsite porphyry Cu-Au (PGE) deposit and ending at ca. 78 Ma in the south at Capitan Dimitrievo.	Southern Panagyurishte district	Krassen HS epithermal Cu-Au (1962-1973)	0.30 Mt @ 0.76% Cu (Strashimirov et al. 2002)
				Petelovo porphyry Au	8.09 Mt @ 0.88 g/t Au (Vassilev and Fargova 1998)
				Radka HS epithermal Cu-Au (1942-1997)	8.9 Mt @ 1.06 % Cu, 1.5 g/t Au, 25 g/t Ag (Moritz et al. 2004)
				Tsar Assen porphyry Cu (1980-1995)	6.6 Mt @ 0.47 % Cu (Strashimirov et al. 2002)
				Elshitsa HS epithermal Cu-Au (1922-1999)	4.5 Mt @ 1.13% Cu, 1.5 g/t Au and 15 g/t Ag (Moritz et al. 2004)
				Vlaykov Vruh porphyry Cu (1962-1979)	mined out 9.793 Mt @ 0.46% Cu; reserves 22 700 t @ 0.32% Cu (Strashimirov et al. 2003)

Abbreviations: HS - high-sulphidation

HS high sulfidation

The Elshitsa volcano-intrusive complex

The Late Cretaceous Elshitsa complex in the Southern Panagyurishte district is a volcano-plutonic structure composed of the volcanic rocks of the Elshitsa effusive formation and the Elshitsa pluton, as well as numerous subvolcanic and subvolcanic–hypabyssal minor intrusions and dykes (Fig. 2a; Bogdanov et al. 1970b; Ignatovski et al. 1990; Popov 2001). *The Elshitsa effusive formation* outcrops in two narrow NW-SE elongated strips on both sides of the Elshitsa intrusion. It comprises a lower andesitic and an upper dacitic units. Lava and coarse-grained pyroclastic rocks of the two units are gradually replaced by lapilli and ash tuffs to the northeast and southwest (Popov 2001).

The Elshitsa pluton was described first as part of a larger composite intrusive body called Elshitsa–Boshulia intrusive by Boyadjiev and Chipchakova (1962), but Ivanov et al. (2002) considered it as a separate, single magmatic body within a subequatorially elongated chain of intrusions of granitic composition parallel to the Iskar–Yavoritsa shear zone (IYSZ). The intrusion is NW-SE elongated (~N120). According to Boyadjiev and Chipchakova (1962), the pluton was formed during multiple magma pulses with varying compositions—an early gabbroic phase, followed by the emplacement of granitic magma, thus producing some hybrid rock varieties. Based on major and trace element geochemistry, Daieva and Chipchakova (1997) and Kamenov et al. (2007) inferred mixing and fractional crystallization processes to explain the compositional varieties in the Elshitsa pluton. Based on their structural, petrological, and magnetic (AMS) features (Ivanov et al. 2002) and on radiogenic isotope geochemistry and U–Pb dating (Peytcheva et al. 2008), the mafic and felsic magmas in the Boshulia intrusive (south of Elshitsa) were interpreted as products of mingling and mixing processes in a differentiated magma chamber. Georgiev and Lazarova (2003) proposed a relatively shallow level of crystallization for the Elshitsa pluton at 750°C and 3.2 kbar, corresponding to a depth of 9 km, compared to the deeper Boshulia pluton (depth of crystallization up to 18–19 km, based on hornblende barometry). Handler et al. (2004) reported an 84.07±0.54 Ma $^{40}Ar/^{39}Ar$ age for magmatic amphibole from the Elshitsa granodiorite.

The subvolcanic and hypabyssal intrusions and dykes were described by Boyadjiev and Chipchakova (1965) as an independent dyke system postdating the emplacement of the Elshitsa pluton. These rocks intruded the Upper Cretaceous volcanic rocks, as well as the Elshitsa pluton and the pre-Mesozoic basement (Fig. 2a). The subvolcanic bodies are subvertical, dacitic to rhyodacitic in composition and have a nearly linear–tabular shape. They are subparallel

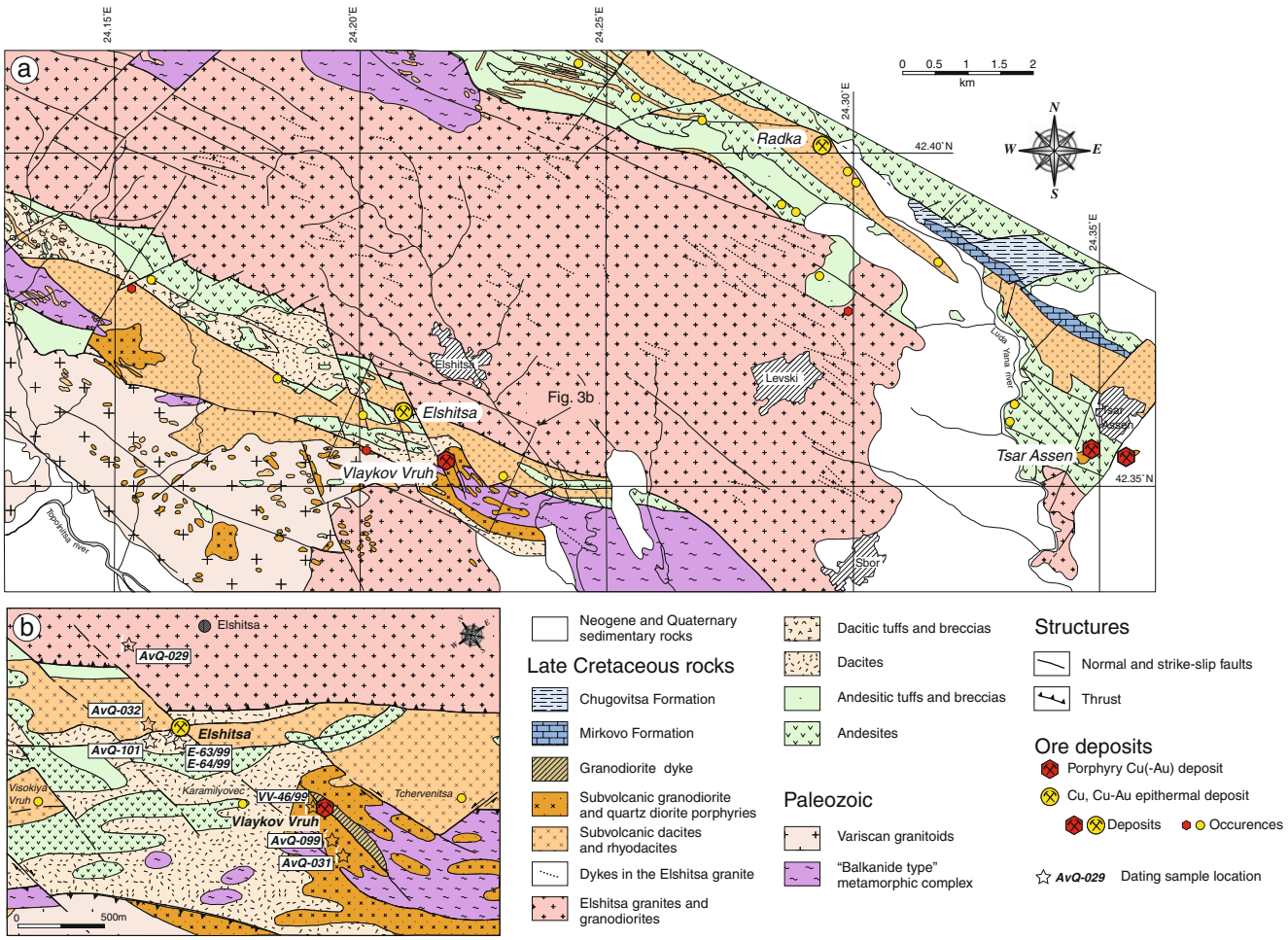

Fig. 2 **a** Geological map of the southern part of the Panagyurishte district (modified after Ignatovski et al. 1990); **b** Geological map of the area of Vlaykov Vruh and Elshitsa deposits (modified after Bogdanov et al. 1970b) with location of the samples used for U–Pb dating

to the contacts of the Elshitsa pluton (~N120) and crop out within both the Elshitsa and the Radka volcanic strips (Fig. 2a). The subvolcanic–hypabyssal intrusions are predominantly granodioritic in composition, with variations to plagiogranite and granite porphyries. They host the porphyry-style mineralization in the southern part of the Panagyurishte district (Kolkovski et al. 1977; Ignatovski et al. 1990; Popov 2001). The Vlaykov Vruh porphyry is the largest intrusion of this type.

As a result of the volcanic and tectonic activities, the Elshitsa magmatic complex was fragmented into four individual blocks (Fig. 2a; Popov 2001): (1) a central block limited by the Stefancho fault to the north and the Elshitsa fault to the south, uplifted by more than 1,500 m, so that the Elshitsa pluton and the basement metamorphic rocks presently crop out at the same hypsometric level as the extrusive products of the Elshitsa stratovolcano; (2) volcanic rocks covered by the Chugovitsa and Mirkovo Formations are preserved in the northern block; (3) a southern block consisting of a narrow volcano-tectonic graben (Elshitsa graben) formed along a series of subparallel faults; and (4) a block occupying the southernmost part of the area, where basement lithologies and the Late Cretaceous Boshulia intrusion are in a highly uplifted position.

Geology of the Vlaykov Vruh porphyry Cu and the Elshitsa epithermal Cu–Au deposits

Among the different paired porphyry Cu and epithermal Cu–Au deposits in the Panagyurishte district, such as Chelopech–Elatsite (in the north part; Chambefort et al. 2007); Petelovo–Krassen (in the central part), Popovo Dere–Kaleto (in the south part; Ignatovski and Bayraktarov 1996), the Elshitsa epithermal Cu–Au deposit and the less than 1 km distant SE Vlaykov Vruh porphyry Cu deposit constitute the best example of the intimate spatial association of high-sulfidation epithermal and porphyry Cu

Fig. 3 View looking southwest toward the Vlaykov Vruh and Elshitsa deposits

systems in the district (Figs. 2b and 3). The two deposits are located along diagonal WNW-striking faults (Fig. 2b), which most probably played an important role for the lateral migration of the mineralizing fluids. Despite the fact that the two mineralization styles, occurring presently at the same crustal level, were formed at different P-T conditions, there is no evidence for any important vertical displacement between the two deposits. Due to their textural and geochemical similarities and field observations, the hypabyssal granodiorite intrusion hosting the Vlaykov Vruh porphyry deposit can be regarded as a deeper analogue of the subvolcanic dacite partially hosting the epithermal ores at Elshitsa (Bogdanov et al. 1972b; Ignatovski et al. 1990). Kouzmanov et al. (2003) provided stable isotope evidence in favor of the close genetic relationship between the two systems, both being formed by oxidized fluids with almost identical oxygen and sulfur isotopic compositions, and evolving in time from purely magmatic in the early mineralization stages to mixed magmatic–meteoric signatures during the later epithermal stage.

The Vlaykov Vruh porphyry Cu deposit

Geology The Vlaykov Vruh deposit is one of the smallest porphyry Cu deposits in the Panagyurishte district (Table 1). The porphyry–copper mineralization is mainly hosted by a granodioritic to quartz–monzodioritic stock (Figs. 4a and 5a). The intrusion was emplaced along the contact between the southern parts of the Elshitsa effusive

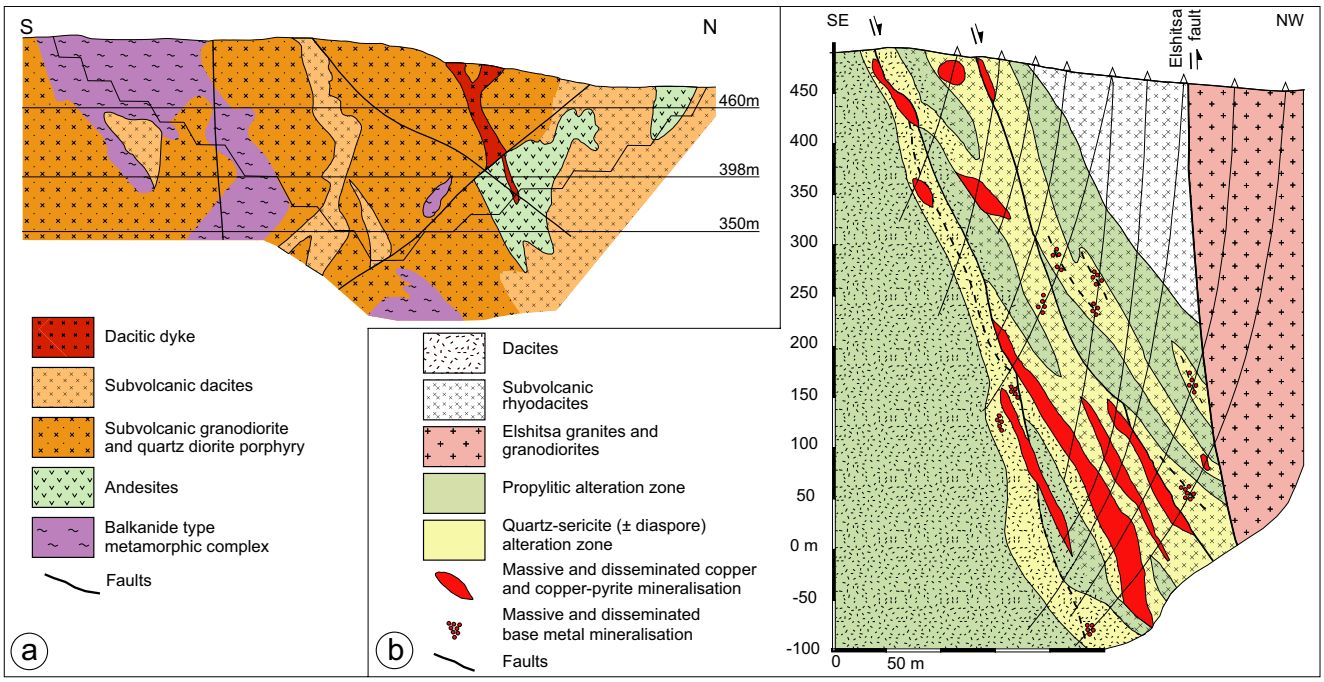

Fig. 4 **a** Cross-section of the Vlaykov Vruh porphyry Cu deposit (after Strashimirov et al. 2003). Open pit outline as of 1979; **b** Cross-section of the Elshitsa epithermal Cu–Au deposit (after Chipchakova and Stefanov 1974)

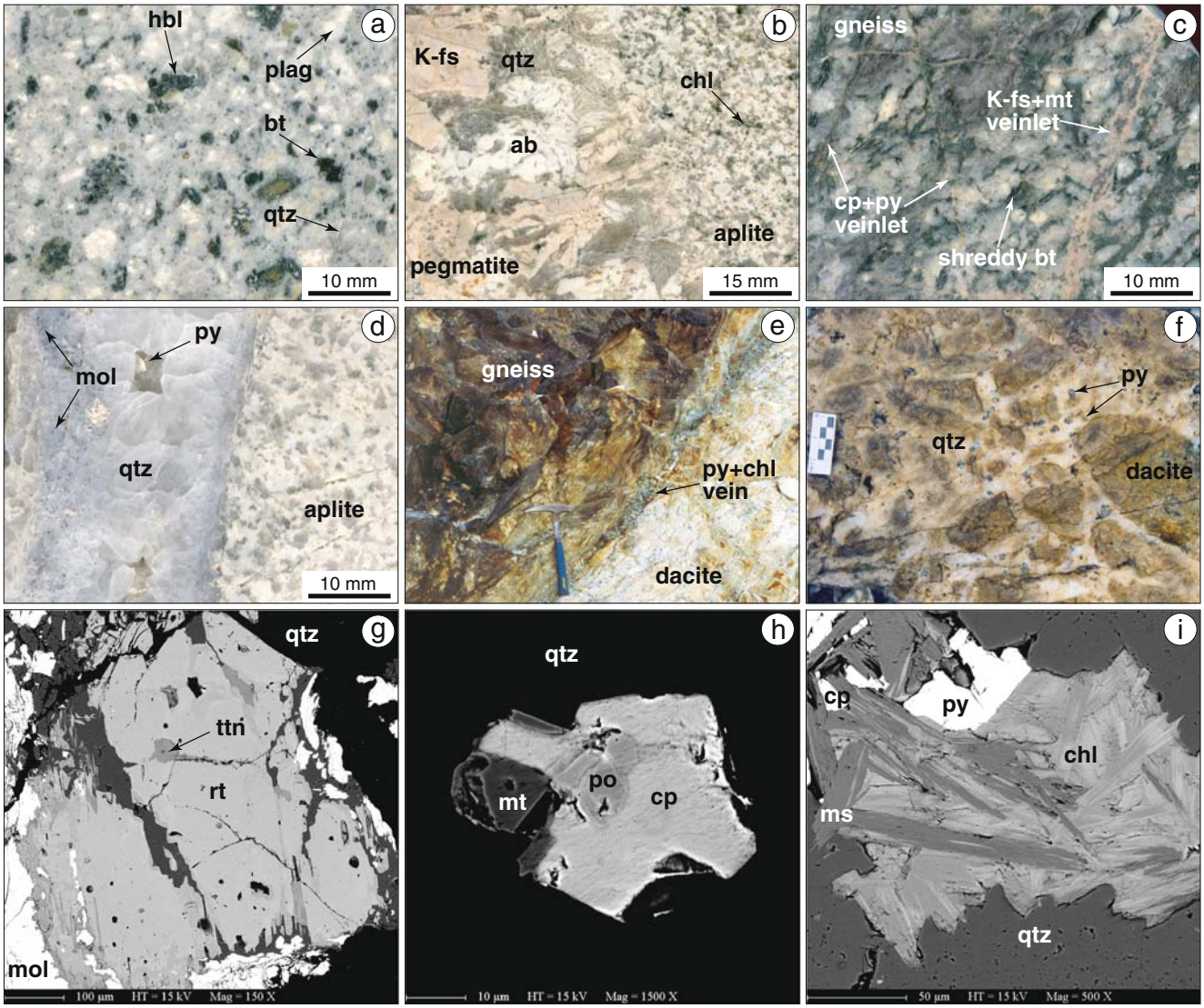

Fig. 5 Ore textures and mineralogy of the Vlaykov Vruh porphyry Cu deposit: **a** Propylitically altered Vlaykov Vruh granodiorite; **b** Aplite–pegmatite texture of felsic dyke cutting the granodiorite porphyry; **c** K-silicate alteration assemblage affecting the host gneisses: shreddy biotite replacing the mafic rocks and K-feldspar–magnetite veinlets cut by later sulfide (chalcopyrite–pyrite) veinlets; **d** Quartz–molybdenite vein with later pyrite crystals in vugs, cutting aplitic dyke; **e** Late pyrite–chlorite vein along the contact between subvolcanic dacitic body and the host gneisses; **f** Hydrothermal breccia cutting subvolcanic dacite. The breccia matrix consists of quartz, pyrite, and minor chlorite and sericite; **g** Hydrothermal rutile from quartz–rutile–molybdenite vein, BSE image; **h** Chalcopyrite–magnetite–pyrrhotite–quartz (± pyrite) association, typical for the main economic mineralization stage at Vlaykov Vruh, BSE image; **i** Pyrite–chalcopyrite–chlorite–muscovite–quartz association from the main economic stage, BSE image. *ab* albite, *bt* biotite, *chl* chlorite, *cp* chalcopyrite, *hbl* hornblende, *K-fs* K-feldspar, *mol* molybdenite, *ms* muscovite, *mt* magnetite, *plag* plagioclase, *po* pyrrhotite, *py* pyrite, *qtz* quartz, *rt* rutile, *ttn* titanite

formation and the pre-Mesozoic metamorphic and granitic basement (Figs. 2b and 4a; Bogdanov et al. 1972a; Strashimirov et al. 2003). The major axis of the intrusion trends N115-120; its length is over 2 km. The intrusion is cut by later dacitic dykes, which were interpreted by Bogdanov et al. (1972b) as ore-controlling. Up to 30-cm large late-magmatic aplite–pegmatite dykes crosscut the intrusion (Fig. 5b). There is no clear evidence for time relationships between the two dyke generations.

Alteration and mineralization The mineral paragenesis of the Vlaykov Vruh deposit displays characteristic features of typical porphyry copper systems (Seedorff et al. 2005) with various generations of quartz–sulfide veinlets formed during successive stages of mineralisation (Fig. 6). According to Strashimirov et al. (2003), the mineralization forms four vertical stockwork ore bodies in the deeper parts, coalescing into a single ore body in the upper part of the deposit. The main ore body was oxidized to a depth of 10–20 m into

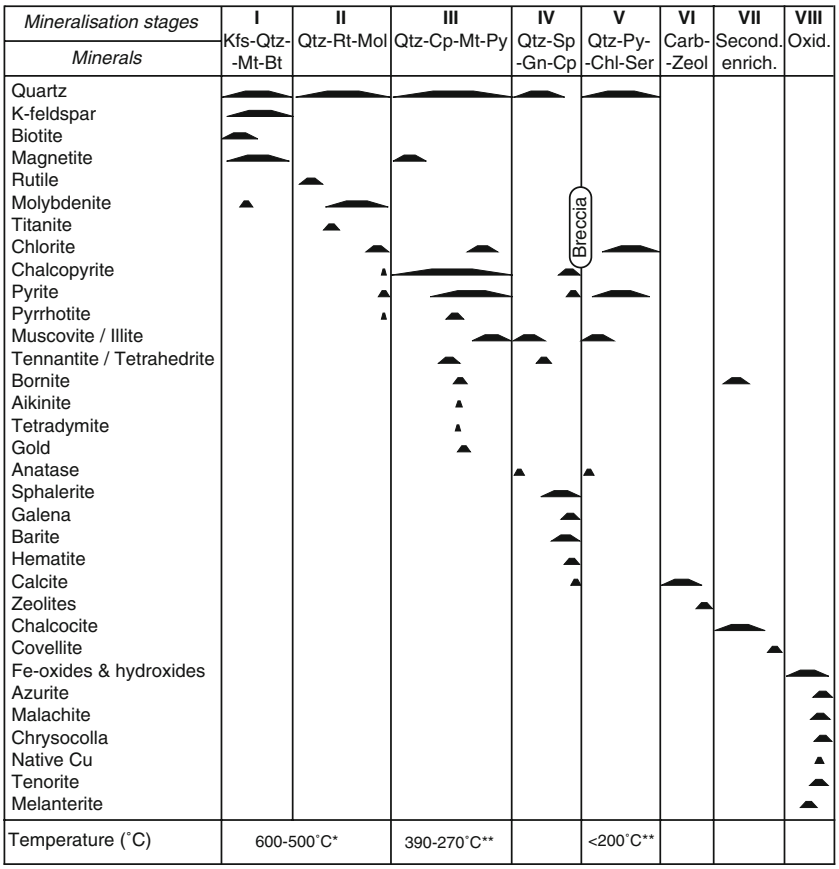

Fig. 6 Paragenetic sequence of the Vlaykov Vruh porphyry Cu deposit (based on Bogdanov et al. 1972b; Popov et al. 2000; Kouzmanov 2001; and Strashimirov et al. 2003). Temperature intervals are based on: (*) Quartz–magnetite O-isotope thermometry (Kouzmanov et al. 2003); and (**) fluid inclusion microthermometry (Popov et al. 2000; Kouzmanov 2001). *Bt* biotite, *Carb* carbonates, *Cp* chalcopyrite, *Gn* galena, *Kfs* K-feldspar, *Mol* molybdenite, *Mt* magnetite, *Py* pyrite, *Qtz* quartz, *Rt* rutile, *Sp* sphalerite, *Zeol* zeolites

malachite–azurite ores, underlain by a 30- to 40-m-thick secondary enrichment zone of bornite–chalcocite–covellite ores (Bogdanov et al. 1972b; Fig. 6). Hypogene alteration including potassic, phyllic, and propylitic alteration zones and mineralization affected all rock varieties in the deposit. The Vlaykov Vruh granodiorite and the two-mica gneiss from the basement underwent potassic alteration (stage I in Fig. 6), leading to the formation of shreddy biotite replacing mafic phenocrysts and the formation of tiny K-feldspar-magnetite veinlets (Fig. 5c). Aplite–pegmatite dykes, located at the southern border of the open pit were propylitically altered and cut by early stage quartz–rutile–molybdenite veins (Fig. 5d; stage II in Fig. 6). Along the western and northwestern border of the open pit, both the relatively late NNW-striking quartz–pyrite veins (Fig. 5e) and the hydrothermal breccias with phyllic alteration (Fig. 5f) show very similar textures to that of the neighboring Elshitsa epithermal deposit (see below). The main economic copper mineralization (stage III in Fig. 6) occurs as tiny veinlets of quartz–chalcopyrite–magnetite ± pyrite ± pyrrhotite or is disseminated (Fig. 5h). Polymetallic veins of quartz–sphalerite–galena–chalcopyrite ± barite (stage IV) were deposited as open-space filling in extensional fractures and were later cut by quartz-pyrite–chlorite veins (stage V; Fig. 5i). The latest hypogene mineral assemblage consists of sporadic carbonate–zeolite veinlets (stage VI).

The Elshitsa epithermal Cu–Au deposit

Geology The Elshitsa epithermal deposit is located in the southeastern part of the Elshitsa volcanic strip and occupies an area of 2–2.5 km length by 0.5–0.7 km width, NW of the Vlaykov Vruh porphyry Cu deposit (Fig. 3). The deposit was one of the first mines that was exploited in the Panagyurishte district, operating from 1922 until 1999. Until the 1960s, the main part of the ore was produced from massive pyrite bodies. For the last 30 years of mining activity, the underground mine production came mainly from copper and/or pyrite–copper–polymetallic bodies. A small open pit was developed in the sector Elshitsa–West in the 1990s. Elshitsa is one of the smallest epithermal deposits in the district (Table 1).

Figure 7 summarizes representative Cu, Au, and Ag ore grades in massive and disseminated pyrite and copper–pyrite bodies at Elshitsa. A good correlation exists between the gold and silver contents of the ore along a 1:5 line

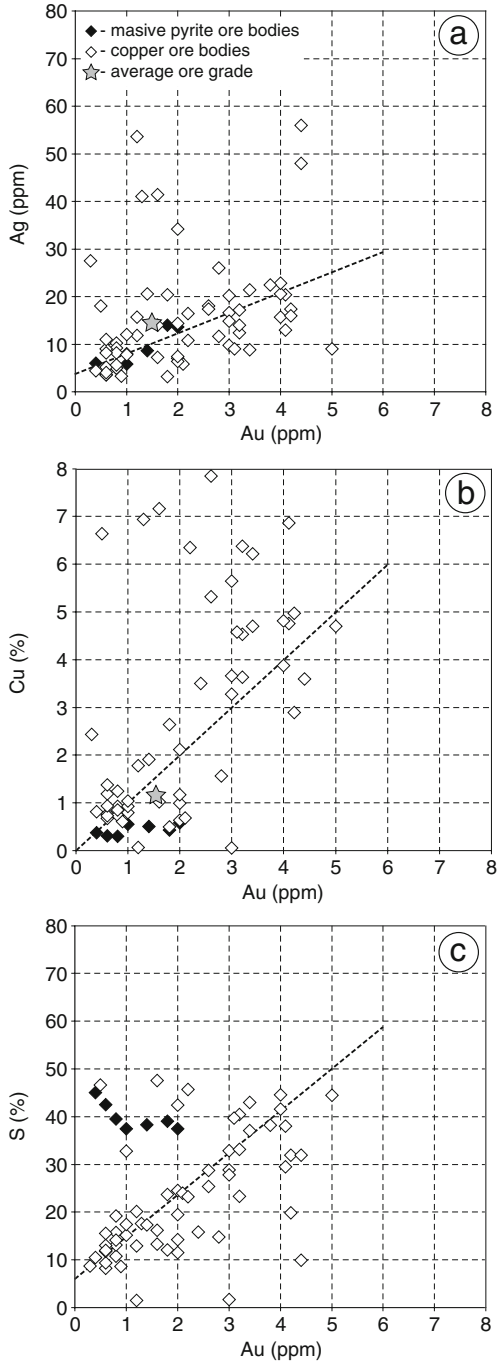

Fig. 7 Gold, silver, and copper ore grades of the Elshitsa epithermal Cu–Au deposit. Data are representative for massive and disseminated pyrite and copper ore bodies from level 80 to level 320: **a** Au (ppm) versus Ag (ppm); **b** Au (ppm) versus Cu (wt %); **c** Au (ppm) versus S (wt.%). The Au, Ag, and Cu average ore grades for the deposit are indicated in (**a**) and (**b**)

(Fig. 7a), with an average Ag/Au ratio of 10, as well as between copper and gold grades along a 1:1 line (Fig. 7b), with an average Cu/Au ratio of 1.3. The gold content in the hypogene ore is usually <5 g/t, mainly in the range 0.5–2 g/t. The copper content usually ranges between 0.5% and 2 %, with values up to 7–8 % in the richest copper bodies. The highest gold grades were registered in the richest copper ore bodies, while the massive pyrite bodies show average gold grades of 0.5–2 g/t (Fig. 7c).

The structure of the deposit is controlled by a subvolcanic dacitic body emplaced along the Elshitsa fault, elongated in NW direction (N110-115) and dipping almost vertically to the NE (75–80°). It cuts an andesitic and dacitic volcanic sequence dipping 10–30° to the north (Bogdanov et al. 1972a). The subvolcanic body is limited by the Elshitsa fault to the north and by an 80- to 120-m-large breccia zone to the south, which is the main host of the epithermal mineralization (Fig. 3b). The latter dips steeply to the NE (65–70°) and is subparallel to the intrusive contact. At depth, it is cut by the Elshitsa fault. More than ten lenticular to columnar massive ore bodies are discordant with respect to the host rock and are structurally controlled by NW-trending normal faults (N110-120), subparallel to the contact of the dacitic subvolcanic body. Massive lens-like bodies generally show tectonic contacts, due to later Alpine reactivation of the main ore-controlling faults (Fig. 8a).

Two compositionally distinct types of ore bodies have been recognized at Elshitsa: (1) massive pyrite, mainly in the eastern sector of the deposit, closer to the Vlaykov Vruh porphyry Cu system, and (2) pyrite–chalcopyrite–quartz or copper–pyrite bodies—mainly in the central and western sectors of the deposit. The latter ore type results from the superposition of a copper-rich mineral paragenesis upon the early massive pyrite ores. In the "Kanata" area, a small gossan (Fig. 8b) developed on the top of one of the massive pyrite bodies and was also mined out in a small open pit. It had a vertical extension of 25–30 m from the surface and total reserves of ~53,000 t with average grades of 7.74 g/t Au and 21.24 g/t Ag.

Bogdanov et al. (1970a) reported massive pyrite clasts in a dacitic breccia matrix from the Radka and Elshitsa deposits (Fig. 8c) and interpreted them as epiclastic rocks resulting from the destruction of massive sulfide ore bodies, suggesting an early ore formation in a shallow water environment coeval with the dacitic volcanism. Kouzmanov et al. (2004) described macro- and microscale polymictic breccia–pipe and breccia–dyke structures with similar pyrite clasts, cutting the massive dacite volcanic rocks as well as the massive ore bodies at Radka, thus suggesting intramineralization formation of the latter due to fluidization of rocks and ore fragments along upward-escaping fluid channelways, which is a common feature to many hydrothermal systems formed in a porphyry-to-epithermal transitional environment (Corbett and Leach 1998).

Replacement textures at Elshitsa are common. Generally, laminated dacitic lapilli tufs are almost entirely replaced by fine-grained pyrite (Fig. 8d). By contrast, only the matrix of

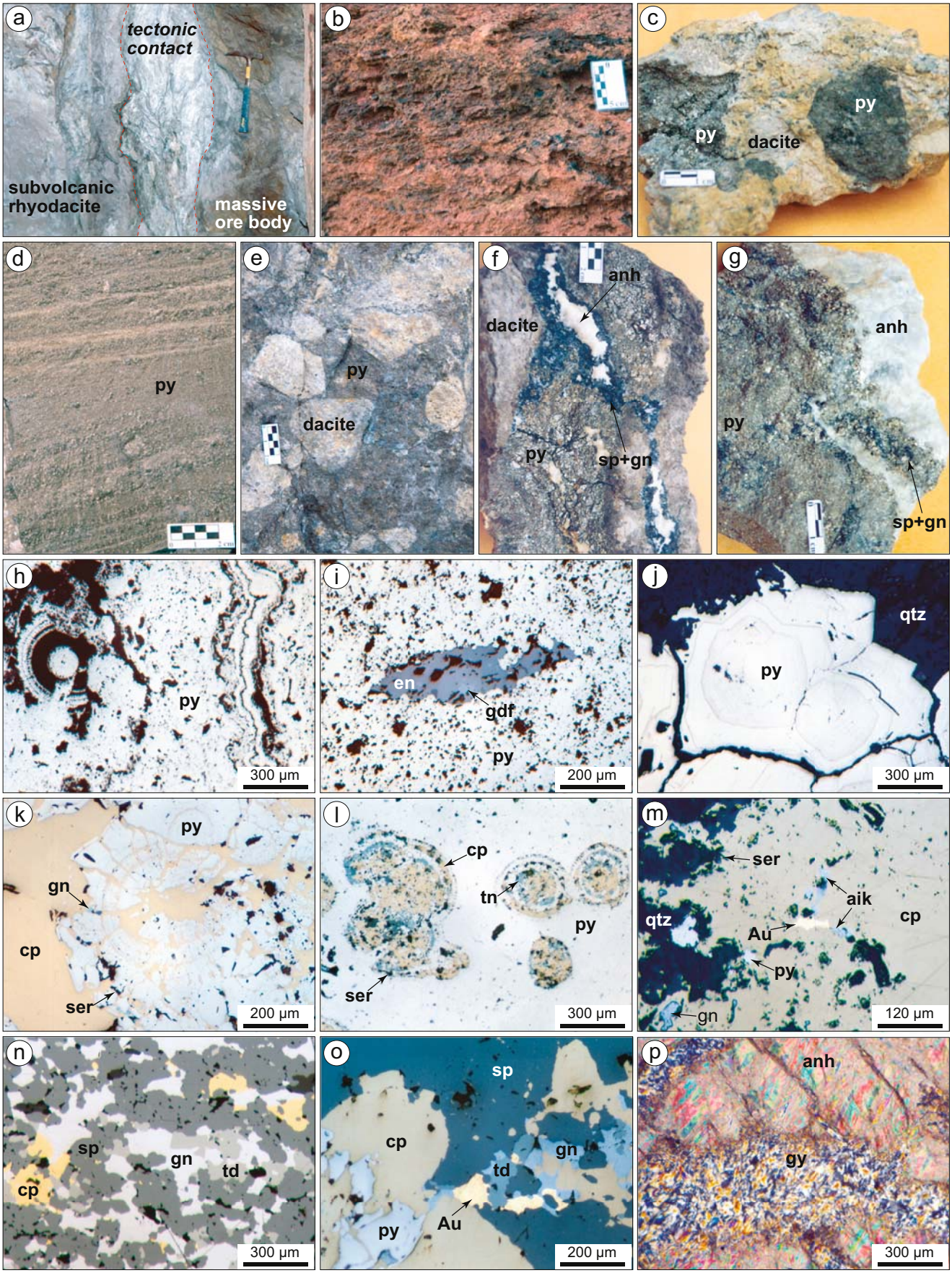
a
tectonic contact
subvolcanic rhyodacite
massive ore body
b
c
py
py
dacite
d
py
e
py
dacite
f
anh
dacite
py
sp+gn
g
anh
py
sp+gn
h
py
300 µm
i
en
gdf
py
200 µm
j
qtz
py
300 µm
k
py
gn
cp
ser
200 µm
l
cp
tn
py
ser
300 µm
m
ser
aik
qtz
cp
Au
py
gn
120 µm
n
sp
gn
td
cp
300 µm
o
sp
cp
gn
td
py
Au
200 µm
p
anh
gy
300 µm

◀ **Fig. 8** Ore textures and mineralogy of the Elshitsa epithermal Cu–Au deposit. Microphotographs are taken in reflected light (//N) except (**p**) which is taken in transmitted light (xN): **a** Tectonic contact of massive copper–pyrite ore body with subvolcanic rhyodacite (level 80; ore body n°1); **b** Boxwork texture typical for the small gossan body developed in the SE part of the Elshitsa deposit; **c** Ore clasts of stage I massive fine-grained pyrite in intramineralization breccia–dyke with fine-grained matrix and clasts of volcanic rhyodacites, tuffs, and subvolcanic dacites; **d** Stage I fine-grained pyrite replacing laminated dacitic ash tuff; **e** Breccia–dyke with hydrothermal matrix (quartz and pyrite) and subrounded dacitic clasts; **f** Vein of stage I pyrite, cut by polymetallic sphalerite–galena vein, with later anhydrite infill; **g** Late anhydrite veins cutting massive pyrite–polymetallic ore; **h** Massive fine-grained and colloform pyrite; **i** Fine-grained pyrite from the massive pyrite bodies, in association with enargite and goldfieldite; **j** Massive coarse-grained As-bearing pyrite. Darker zones correspond to higher As contents. Microphotograph is taken after etching of the polished section with HNO_{3conc}; **k** Stage II chalcopyrite replacing the stage I colloform pyrite; **l** Colloform structures in stage I massive pyrite, selectively replaced by chalcopyrite and tennantite from stage II; **m** Massive chalcopyrite with inclusions of native gold, galena, and aikinite. Quartz and sericite constitute the alteration assemblage; **n** Fine-grained polymetallic ore from the ore stage III: sphalerite, galena, chalcopyrite, and tetrahedrite in various proportions are the dominant minerals; **o** Native gold in association with the main minerals of the polymetallic stage; **p** Supergene gypsum replacing hypogene anhydrite along fractures and cleavage planes. *aik* aikinite, *anh* anhydrite, *Au* gold, *cp* chalcopyrite, *en* enargite, *gdf* goldfieldite, *gn* galena, *gy* gypsum, *py* pyrite, *qtz* quartz, *ser* sericite, *sp* sphalerite, *td* tetrahedrite, *tn* tennantite

the breccia zone bordering the subvolcanic dacite body to the south is replaced by a fine-grained pyrite ± silica assemblage, which preserves subangular to rounded dacite clasts (Fig. 8e). Veins are less abundant, but when present, they provide good textural evidence for time relationship between ore-forming stages (Fig. 8f). The most common textures are the massive ones (Fig. 8g), gradually replaced by disseminated mineralization toward the periphery of the ore bodies.

Alteration and mineralization Wallrock alteration at Elshitsa is structurally and morphologically related to the ore-controlling faults (Fig. 4b). Radonova (1967a, 1967b, 1970) described the alteration zoning in the ore bodies consisting of inner silica-rich zone, phyllic zone with quartz–sericite–pyrite ± diaspore, quartz–sericite zone with dumortierite described at two localities, and an outer zone with chlorite–epidote–albite propylitic assemblage. The ore bodies are typically hosted by the phyllic alteration zone (± diaspore and/or dumortierite). Chipchakova and Stefanov (1974) noted the presence of a $2M_1$ polytype of sericite associated with the early massive pyrite bodies and of lower-temperature 1M polytype associated with the later copper mineralization. In addition to this time-zonation, Kouzmanov (2001) reported a lateral zonation of the polytypes of illite—from $2M_1$-rich zones in the vicinity of the Vlaykov Vruh deposit to 1M-rich zones in the northwestern-most part of the deposit at Elshitsa–West. This illite zonation is most probably related to a temperature trend laterally decreasing away from the intrusion-centered porphyry copper system. Apart from this zonation, Dimitrov (1985) noted the presence of an alunite-bearing advanced argillic zone, around the uppermost level of a major massive pyrite body at Elshitsa.

The epithermal deposits in the Panagyurishte district display numerous paragenetic similarities including: (1) an early massive to disseminated pyrite stage; (2) an intermediate Au-bearing Cu–As–Sn–Bi–S stage; and (3) a later base-metal (Zn–Pb ± Sb, Au) stage (Bogdanov and Bogdanova 1974b; Moritz et al. 2004). The mineral paragenesis at Elshitsa slightly differs from those of typical high-sulfidation epithermal deposits described worldwide (Fig. 9) and even from that of other epithermal Cu–Au deposits in the Panagyurishte district. In the deposit, typical high-sulfidation minerals such as enargite, covellite, and bornite (Einaudi et al. 2003) are much less abundant than at Chelopech, Radka, and Krassen, and advanced argillic and argillic alteration zones are only restricted to the uppermost levels of the system. These features are attributed to a greater depth of epithermal ore formation at Elshitsa, directly linked to the porphyry Cu system at Vlaykov Vruh, and/or to a deeper erosional level in the southern part of the district, compared to the central and northern parts.

The stage I massive pyrite bodies (Fig. 9) mainly consist of fine-grained and colloform pyrite (Fig. 8h), with rare rutile, cassiterite, and covellite inclusions. Enargite and goldfieldite inclusions occur sporadically (Fig. 8i), indicating a high- to very high-sulfidation state of the mineralizing fluids (Einaudi et al. 2003). The early pyrite generation is As-bearing, generally showing oscillatory growth zoning (Fig. 8j). Electrum and gold occur as submicroscopic to rare microscopic inclusions in pyrite, as well as invisible gold in the pyrite structure (Bogdanov et al. 1997). Following the formation of intramineralization breccia–dykes with clasts of massive pyrite, the minerals of the Cu-stage II (Fig. 9) precipitated as replacement of the fine-grained and colloform pyrite of stage I (Fig. 8k and l) or formed separated ore bodies. The Cu–Bi–Te–Pb–As stage II assemblage mainly consists of chalcopyrite, tennantite, and minor sphalerite and galena, with rare As–Sn–Bi-bearing sulfosalts and various Cu–Bi–Au–Ag tellurides (Fig. 9; Kouzmanov et al. 2005). Native gold and electrum occur mainly as inclusions in chalcopyrite (Fig. 8m). Sphalerite–galena–tetrahedrite–chalcopyrite–barite is the main mineral association of the polymetallic stage III (Figs. 8n and 9). It forms narrow veins (Fig. 8f) or selectively replaces the mineral assemblages of the previous mineralization stages. Most of the microscopic gold at Elshitsa is associated with this assemblage

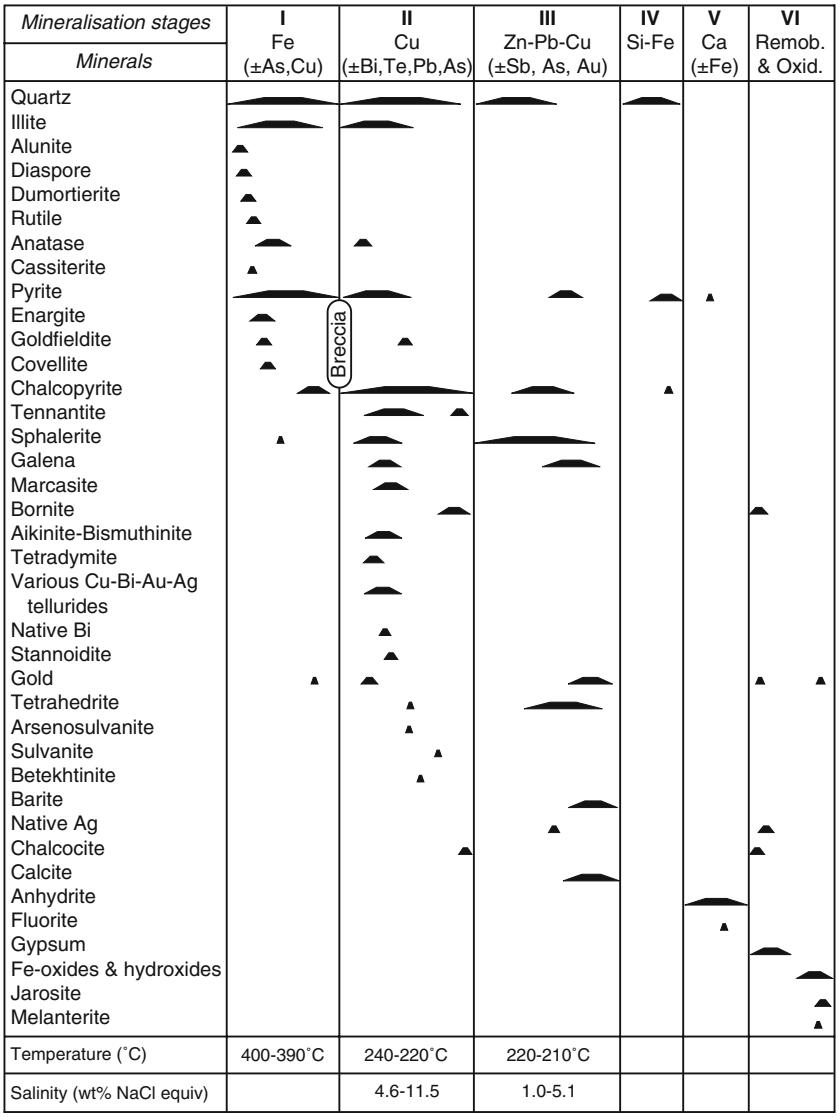

Fig. 9 Paragenetic sequence of the Elshitsa epithermal Cu–Au deposit (based on Popov et al. 2000 and Kouzmanov 2001 and references therein). Temperature intervals are according to Strashimirov and Kovachev (1992) and were determined by fluid inclusion microthermometry. Salinities of the mineralizing fluids are from Kouzmanov (2001)

(Fig. 8o). Bogdanov et al. (1997) reported a progressive increase of the gold fineness from the early massive pyrite to the late polymetallic mineralization stage. Based on the mineral associations, an intermediate sulfidation state can be inferred for the mineralizing fluids of stages II and III (Einaudi et al. 2003). Late massive anhydrite veins (stage V in the paragenetic sequence of Fig. 9) crosscut the earlier formed sulfides (Fig. 8f) and are partially replaced by supergene gypsum in the uppermost parts of the ore bodies (Fig. 8p). Registered temperature and salinity intervals for the mineralizing fluids at Elshitsa (Fig. 9) are typical for high-sulfidation epithermal systems (Arribas 1995).

The Radka epithermal Cu–Au deposit, located in the central part of the Radka volcanic strip (Fig. 2a) shares many common features with the Elshitsa epithermal deposit (Bogdanov and Bogdanova 1974a; Tsonev et al. 2000; Kouzmanov et al. 2002, 2004), therefore several samples of sulfides and sulfates from Radka were also analyzed for comparison in the present study.

Whole rock geochemistry

The analytical techniques used in the present study are summarized in Appendix 1. Major oxide and trace and REE analyses of Late Cretaceous volcanic and intrusive rocks from the southern part of the Panagyurishte district are reported in Appendix 2 and presented in Figs. 10 and 11. Published data for the same area are also plotted for comparison. The TAS diagram (Fig. 10a) illustrates a typical trend for the magmas in the Elshitsa magmatic complex—starting from basaltic and evolving to rhyolitic

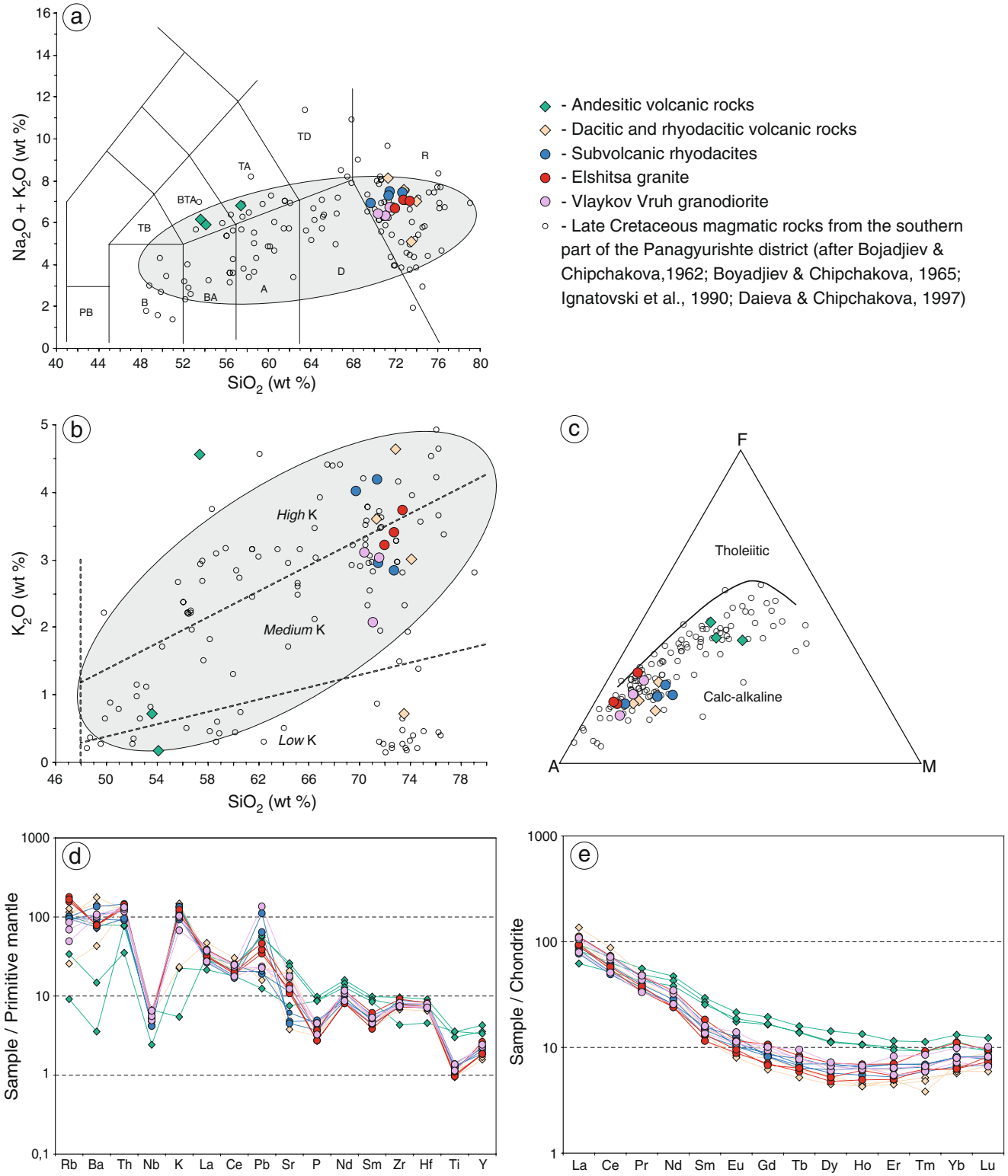

Fig. 10 Major and trace element composition of unaltered Late Cretaceous volcanic and intrusive rocks from the southern part of the Panagyurishte district. Data from this study are presented in *color*, and published data are presented as *open dots*: **a** ($Na_2O + K_2O$) versus SiO_2 (TAS diagram; division after Le Maitre et al. 1989). Data from Appendix 2 are used after normalization to 100% of the ten major oxides. The *gray field* shows the general trend for the Southern Panagyurishte magmas; **b** K_2O versus SiO_2 diagram (division after Le Maitre et al. 1989). Most of the igneous rocks from the southern part of the district plot within the medium-K and high-K fields; **c** AFM diagram (division after Kuno 1968); **d** Trace element concentrations normalized to the primitive mantle composition (after Sun and McDonough 1989); **e** Rare earth element abundances normalized to chondritic meteorite values (after McDonough and Sun 1995)

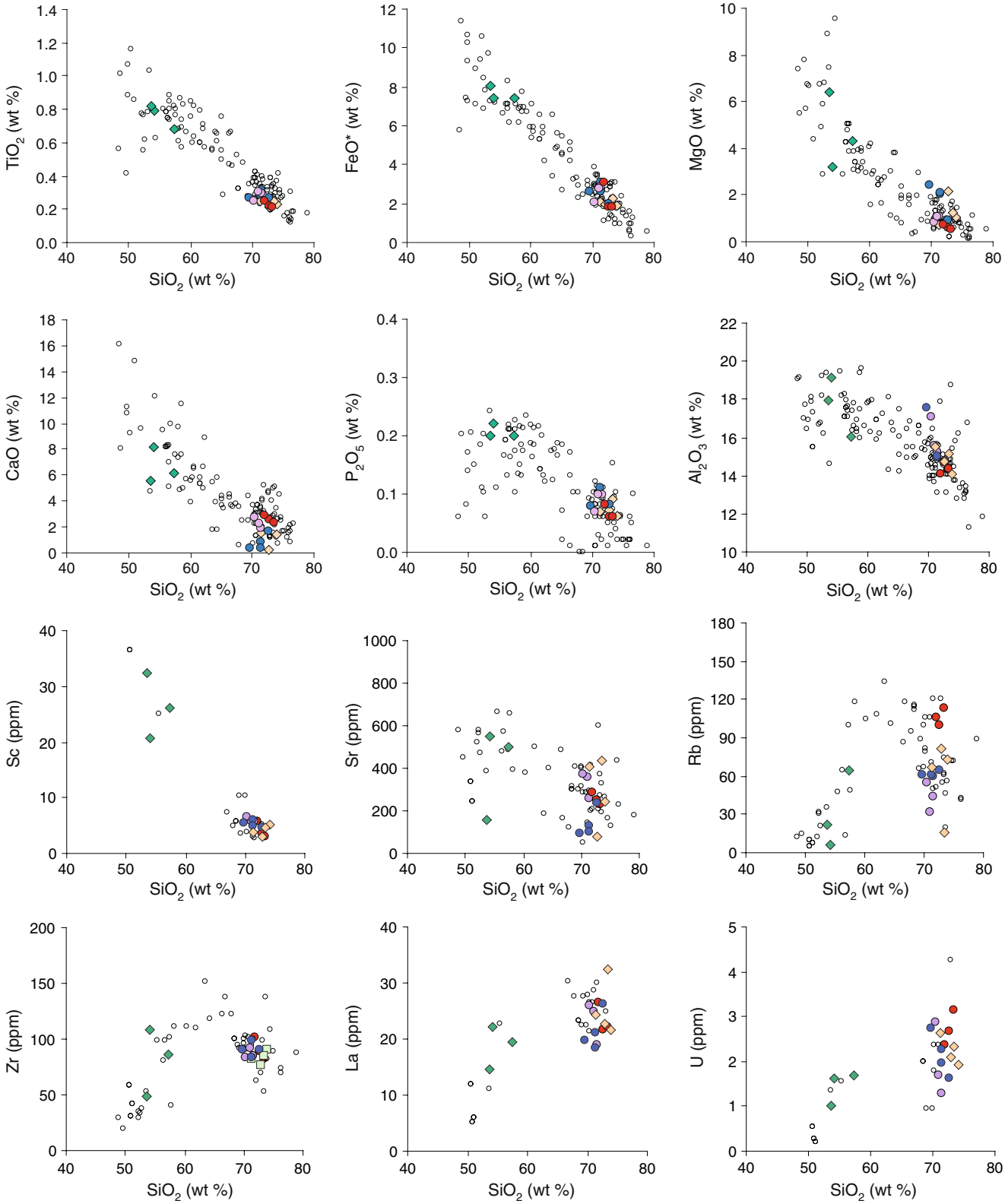

Fig. 11 Variation of wt.% TiO_2, FeO*, MgO, CaO, P_2O_5, and Al_2O_3, and ppm Sc, Sr, Rb, Zr, La, and U versus wt.% SiO_2 for Late Cretaceous volcanic and intrusive rocks from the Elshitsa magmatic complex. Symbols—as in Fig. 10

compositions, with few data plotting in the trachytic field. Most of the igneous rocks plot within the medium- and high-K fields in the K_2O versus SiO_2 diagram (Fig. 10b). The K_2O/Na_2O ratio varies between 0.2 and 2.1, but in most cases is <0.8. The igneous rocks from Southern Panagyurishte district define a typical calc-alkaline trend on the AFM diagram (Fig. 10c).

All studied rocks show similar incompatible trace element patterns (Fig. 10d) with an enrichment of large-ion lithophile elements (LILE: K, Rb, Ba, Pb) and depletion of high field strength elements (HFSE: Nb and Ti), which are typical features of magmas from convergent margin tectonic settings (Saunders et al. 1980). For two of the andesite and one of the rhyodacite samples, concentrations of mobile elements (Rb, Ba, and K) have been most probably affected by a hydrothermal overprint, even if in thin sections only minerals typical for the propylitic alteration assemblage have been observed. Consistent differences in the trace-element pattern between andesites and more felsic varieties can be observed (Fig. 10d).

Chondrite-normalized REE patterns of studied rock varieties are presented in Fig. 10e. Felsic rocks (rhyodacites including subvolcanic varieties, Vlaykov Vruh granodiorite, and Elshitsa granite) show very similar REE patterns, with a moderate light REE enrichment, and a flat (andesites) to slightly concave (felsic rocks) heavy REE portion. All studied rocks from the Elshitsa magmatic complex are characterized by an absence of Eu anomaly.

As shown in Harker variation diagrams (Fig. 11), most of the igneous rocks from the Elshitsa magmatic complex form near-linear to curvilinear trends with decreasing TiO_2, FeO*, MgO, CaO, and P_2O_5 concordant with increasing SiO_2. The marked inflections of some patterns at approximately 55 wt.% SiO_2 suggest fractionation of olivine, hornblende, a Ti-bearing phase (possibly magnetite), apatite, and clinopyroxene during the process of magmatic crystallization. Extensive plagioclase fractionation most probably did not take place, as indicated by the absence of any Eu anomaly and negative Sr–SiO_2 correlation. The strong decrease of Al_2O_3 and Rb (± K_2O) detected in the felsic compositions is most probably due to K-feldspar fractionation at approximately 65–70 wt% SiO_2. The very similar curvilinear pattern of Zr, La, and U suggests strong zircon fractionation at approximately 70 wt.% SiO_2, typical for felsic magmas. Fractionation of La at this composition in parallel with a decrease of CaO could be also indicative for apatite fractionation.

Radiogenic (Pb, Sr, Nd) isotope geochemistry

Lead isotope data for whole-rock samples from the southern part of the Panagyurishte district are plotted in Fig. 12a and b. For all samples, [U], [Th], and [Pb] were measured, and the ratios corrected at 85 Ma for in situ produced radiogenic Pb. The range of initial values for Late Cretaceous igneous rocks is $^{206}Pb/^{204}Pb$=18.13–18.64, $^{207}Pb/^{204}Pb$=15.58–15.64, and $^{208}Pb/^{204}Pb$=37.69–38.56 (Table 2). Basement lithologies, including gneisses and Variscan intrusions, plot within the trends defined by Late Cretaceous igneous rocks. One sample of a Turonian sedimentary rock displays the most radiogenic composition within the studied suite of rocks. Within the Late Cretaceous rocks, the subvolcanic rhyodacites display the largest data scatter, while the data from the Vlaykov Vruh granodiorite, together with the Elshitsa granite, and andesites and rhyodacites form a tighter cluster. On the $^{208}Pb/^{204}Pb$ versus $^{206}Pb/^{204}Pb$ diagram (Fig. 12a), Late Cretaceous igneous rocks define a well-expressed trend overlapping and subparallel to the orogenic and upper crust growth curves of Zartman and Doe (1981). On the $^{207}Pb/^{204}Pb$ versus $^{206}Pb/^{204}Pb$ diagram (Fig. 12b), our data points overlap with the orogenic growth curve or plot in a trend subparallel to it. Our whole-rock lead isotope data indicate Pb from mixed crustal–mantle or dominantly crustal sources. These data are partially overlapping with the trend of von Quadt et al. (2005) for Late Cretaceous igneous rocks from a north–south profile across the whole Panagyurishte district. Both trends crosscut the field of Variscan intrusions, defined by the data of Amov et al. (1973). Age-uncorrected data for gneisses from the Central Srednogorie (Amov et al. 1982) are also presented on the diagrams for comparison.

Lead isotopic compositions of sulfides from different mineralization stages in the Elshitsa and Radka epithermal and Vlaykov Vruh porphyry Cu deposits are listed in Table 3 and plotted in Fig. 12c and d together with the data of Amov et al. (1974). The data points form a well-differentiated cluster ($^{206}Pb/^{204}Pb$=18.432–18.534, $^{207}Pb/^{204}Pb$=15.608–15.647, and $^{208}Pb/^{204}Pb$=37.497–38.630), approximately within the analytical error. Only one sample of pyrite from a gneiss-hosted quartz–chalcopyrite–pyrite porphyry vein at Vlaykov Vruh shows a lower $^{206}Pb/^{204}Pb$ ratio. There is no correlation between stages of mineralization and Pb isotopic composition of ore minerals from Elshitsa, Radka, and Vlaykov Vruh. Ore samples from the Southern Panagyurishte district plot within the same range of $^{206}Pb/^{204}Pb$ ratios as the host Late Cretaceous intrusive and volcanic rocks, with slightly more radiogenic $^{207}Pb/^{204}Pb$ and $^{208}Pb/^{204}Pb$ compositions. Lead isotopic compositions of ore minerals from epithermal and porphyry Cu (–Au) deposits from the Central and Northern Panagyurishte are plotted in Fig. 12c and d for comparison (see "Discussion" section below).

Strontium isotope analyses of various basement lithologies and Late Cretaceous igneous and sedimentary rocks

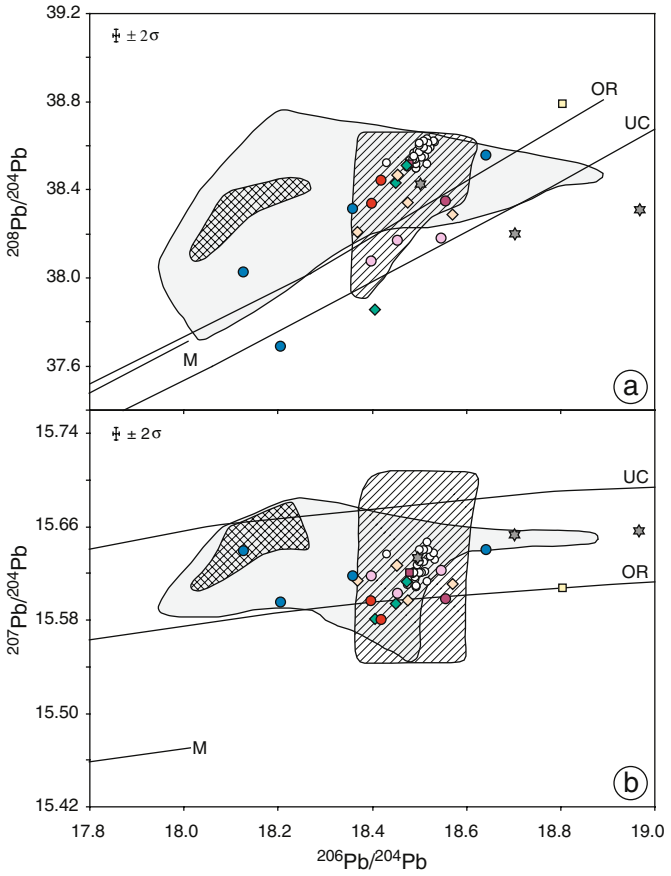

- Vlaykov Vruh granodiorite
- Elshitsa granite
- Subvolcanic rhyodacite
- Volcanic rhyodacite
- Volcanic andesite
- Turonian marl
- Variscan intrusion
- Two-mica gneiss
- Vejen granite - Variscan intrusion in Northern Panagyurishte (data from von Quadt et al. 2005; corrected for 90 Ma)
- Late Cretaceous igneous rocks from Central Srednogorie (data from von Quadt et al. 2005; corrected for 90 Ma)
- K-feldspars from pegmatites in Variscan intrusions from Central Srednogorie (data from Amov et al. 1973)
- Gneisses from Central Srednogorie (data from Amov et al.,1982)
- Ore samples from Vlaykov Vruh, Elshitsa and Radka deposits (data from this study and Amov et al.1974)

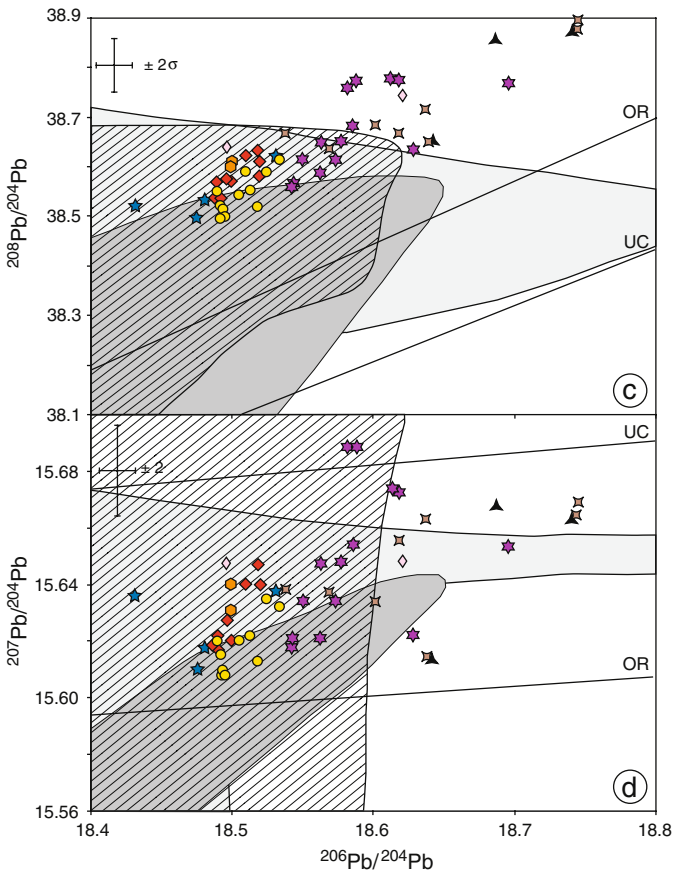

Epithermal and porphyry Cu-Au deposits from the Panagyurishte district:

North

- Elatsite porphyry (Moritz et al. 2001; von Quadt et al. 2002)
- Chelopech epithermal (Moritz et al. 2001)
- Medet porphyry (Moritz et al. 2001)
- Assarel porphyry (Amov et al. 1974; Moritz et al. 2001)
- Krassen epithermal (Amov et al. 1974)
- Radka epithermal (this study; Amov et al. 1974)
- Elshitsa epithermal (this study; Amov et al. 1974)
- Vlaykov Vruh porphyry (this study; Amov et al. 1974)

South

- Late Cretaceous igneous rocks from the southern part of the Panagyurishte district (this study; corrected for 85 Ma)

◀ **Fig. 12** **a** $^{208}Pb/^{204}Pb$ versus $^{206}Pb/^{204}Pb$ and **b** $^{207}Pb/^{204}Pb$ versus $^{206}Pb/^{204}Pb$ plots of whole rocks from the Southern Panagyurishte district. Data for the Variscan Vejen granite, K-feldspars from pegmatites in other Variscan intrusions from Central Srednogorie, gneisses from Central Srednogorie, and ores from Vlaykov Vruh, Elshitsa, and Radka deposits are presented for comparison. All Pb isotope data have been age corrected (85 Ma; von Quadt et al. 2005—for 90 Ma), except the Pb data of Amov et al. (1973, 1982); **c** $^{208}Pb/^{204}Pb$ versus $^{206}Pb/^{204}Pb$ and **d** $^{207}Pb/^{204}Pb$ versus $^{206}Pb/^{204}Pb$ plots of sulfide ore minerals from the Panagyurishte district. The evolution curves of the mantle (M), upper crust (UC), and orogen (OR) are from Zartmann and Doe (1981)

from the southern part of the Panagyurishte district are given in Table 4. After age correction for 85 Ma, initial strontium isotope data were reported in Fig. 13 together with some published data for the southern and northern parts of the district. $^{87}Sr/^{86}Sr$ ratios for basement lithologies range from 0.70846 to 0.71600. In the northern part of the district, the basement metamorphic rocks have $^{87}Sr/^{86}Sr$ ratios from 0.7090 up to 0.7329 (90 Ma age correction). Late Cretaceous sedimentary rocks, including a pre-magmatic Turonian marl, and marls from the Mirkovo and Chugovitsa Formations, yield very similar $^{87}Sr/^{86}Sr$ ratios that fall within the range of Late Cretaceous seawater $^{87}Sr/^{86}Sr$ ratios (Koepnick et al. 1985). Data points for Late Cretaceous igneous rocks from Southern Panagyurishte plot within a restricted interval of 0.70464 to 0.70612. The Elshitsa granite, representing the plutonic part of the Elshitsa magmatic complex, has a less radiogenic composition and clearly differs from the Vlaykov Vruh granodiorite, andesites and rhyodacites, including subvolcanic varieties (Fig. 13). There is no significant correlation among the initial $^{87}Sr/^{86}Sr$ ratio and SiO_2 content (Fig. 14a), neither with Sr and Rb concentration, nor with the Rb/Sr ratio.

The initial $^{143}Nd/^{144}Nd$ ratios for Late Cretaceous igneous rocks range from 0.51241 to 0.51255 (Table 4). On the SiO_2 versus $^{143}Nd/^{144}Nd_i$ diagram, the Southern Panagyurishte magmas plot between the well-defined field of the Banatitic rocks of South Romania (Dupont et al. 2002), which are the most radiogenic and the Chelopech magmas (Stoykov et al. 2004), which show the least radiogenic composition (Fig. 14b).

In a $^{87}Sr/^{86}Sr_{(i)}$ versus $^{143}Nd/^{144}Nd_{(i)}$ diagram (Fig. 14c), the Southern Panagyurishte Late Cretaceous magmatic rocks lie on the mantle array and form a cluster between the EM-I and EM-II fields (Fig. 14c). Such data distribution could be due to primary magma source differences and/or contamination of mantellic magmas by crustal materials at middle/upper crustal levels. In comparison with the Chelopech magmas and the Capitan Dimitrievo pluton, our samples show more radiogenic Sr isotopic signatures and Nd isotopic compositions intermediate between the two (Fig. 14c).

Carbonates and sulfates precipitated relatively late in the evolution of the hydrothermal systems in the southern part of the Panagyurishte district (Figs. 6 and 9). The strontium isotopic compositions of hydrothermal barite (Elshitsa, Radka, and Vlaykov Vruh deposits), calcite (Elshitsa), and anhydrite (Elshitsa and Radka) fall between the Sr isotopic composition of the basement rocks and the one of the Late Cretaceous magmatic rocks partially overlapping the range of the latter (Fig. 13). They range from 0.70581 to 0.70729 (Table 5, Fig. 13). One sample of barite from the Vlaykov Vruh deposit has a composition very similar to the initial $^{87}Sr/^{86}Sr$ ratio of the host granodiorite intrusion. Two calcite samples from the polymetallic stage III in Elshitsa yield less radiogenic $^{87}Sr/^{86}Sr$ ratios than cogenetic barite. Anhydrite from the Elshitsa and Radka epithermal deposits shows the largest scatter in composition. Compared to Late Cretaceous seawater and Upper Cretaceous marls from the Southern Panagyurishte, hydrothermal sulfates and carbonates have less radiogenic composition.

The Sr concentration of anhydrite from the Elshitsa and Radka deposits covaries with its $^{87}Sr/^{86}Sr$ ratio (Fig. 15a) and yields a linear trend that is explained by mixing of fluids from different sources during the late stages of ore formation in the epithermal deposits. The hypothetical end-member fluids are attributed to: (a) a Sr-rich and radiogenic fluid source, and (b) a Sr-poor and less radiogenic fluid source (Fig. 15a). Extensive fluid circulation through basement lithologies (metamorphic rocks, Variscan granites, and/or Turonian sedimentary rocks) could explain type (A) fluid, while type (B) fluid can be generated by fluid circulation through the Late Cretaceous igneous rocks or could simply represent Late Cretaceous magmatic ore fluid. To better constrain the origin of the late-stage anhydrite-precipitating fluids in the epithermal deposits from the Southern Panagyurishte, their $\delta^{18}O$ value (Kouzmanov et al. 2003) has been plotted with respect to the $^{87}Sr/^{86}Sr$ composition of the studied anhydrite samples (Fig. 15b). The few analytical points fall between the isotopic composition of local meteoric water and the isotopic composition of primary magmatic water, thus suggesting anhydrite precipitation from isotopically exchanged meteoric fluids or most probably from mixed oxidized magmatic and meteoric fluids. No relationship between anhydrite precipitation and Senonian seawater can be inferred based on Fig. 15b.

U–Pb geochronology

Five samples of Late Cretaceous igneous rocks hosting the Elshitsa and Vlaykov Vruh deposits have been used for the U–Pb geochronological study (Fig. 2b). They come from the Elshitsa granite (AvQ 029), a subvolcanic rhyodacite

Table 2 Pb, U, and Th concentrations, measured Pb isotopic ratios and calculated Pb initial ratios of whole rock samples from the southern part of the Panagyurishte district

Sample	Rock type	Pb (ppm)	U (ppm)	Th (ppm)	$^{206}Pb/^{204}Pb$ measured	$^{207}Pb/^{204}Pb$ measured	$^{208}Pb/^{204}Pb$ measured	$^{206}Pb/^{204}Pb_i$ (t=85Ma)	$^{207}Pb/^{204}Pb_i$ (t=85Ma)	$^{208}Pb/^{204}Pb_i$ (t=85Ma)
E 60/99	Two-mica gneiss	125	3.6	21	18.505	15.622	38.561	18.48	15.62	38.51
E 17/00	Variscan granite	5.6	2.0	6.1	18.855	15.612	38.648	18.56	15.60	38.35
E 19/00	Turonian marl	10.7	1.3	4.6	18.905	15.612	38.906	18.80	15.61	38.79
E 20/00	Andesite	10.3	1.6	6.5	18.606	15.620	38.686	18.47	15.61	38.51
R 01/00	Andesite	10.7	1.7	6.7	18.581	15.601	38.602	18.45	15.59	38.43
E 53/99A	Andesite	2.3	1.0	3.0	18.776	15.599	38.212	18.40	15.58	37.86
E 53/99B	Rhyodacite	11.8	1.9	10.8	18.591	15.634	38.717	18.45	15.63	38.47
R 17/99	Rhyodacite	7.2	2.1	11.2	18.720	15.609	38.768	18.48	15.60	38.34
VV 35/99	Rhyodacite	4.3	2.6	10.6	18.885	15.638	38.891	18.37	15.61	38.21
R 19/99	Rhyodacite	2.9	2.3	10.5	19.248	15.643	39.284	18.57	15.61	38.29
VV 36/99	Subvolcanic rhyodacite	3.5	1.6	12.4	18.591	15.613	38.645	18.21	15.59	37.69
E 52/99	Subvolcanic rhyodacite	3.8	2.3	9.9	18.864	15.642	39.041	18.36	15.62	38.31
E 66/99	Subvolcanic rhyodacite	11.9	2.0	7.7	18.782	15.647	38.736	18.64	15.64	38.56
AvQ 032	Subvolcanic rhyodacite	2.6	1.9	8.1	18.739	15.668	38.895	18.13	15.64	38.03
E 16/97	Elshitsa granite	6.4	2.7	11.5	18.752	15.614	38.837	18.40	15.60	38.34
AvQ 029	Elshitsa granite	12.3	2.5	9.0	18.585	15.588	38.642	18.42	15.58	38.44
VV 06/99	Vlaykov Vruh granodiorite	4.4	1.3	10.0	18.698	15.615	38.796	18.46	15.60	38.17
VV 23/99	Vlaykov Vruh granodiorite	4.2	1.7	10.8	18.885	15.639	38.891	18.55	15.62	38.18
AvQ 031	Vlaykov Vruh granodiorite	3.4	2.0	11.3	18.892	15.641	38.992	18.40	15.62	38.07

2σ error: $^{206}Pb/^{204}Pb$=0.006; $^{207}Pb/^{204}Pb$=0.006; $^{208}Pb/^{204}Pb$=0.031

Table 3 Pb isotopic compositions of ore minerals from the Elshitsa, Radka, and Vlaykov Vruh deposits

Sample	Deposit	Mineral	Mineralisation stage	$^{206}Pb/^{204}Pb$	$^{207}Pb/^{204}Pb$	$^{208}Pb/^{204}Pb$
E 58/97	Elshitsa	py	Stage I	18.493	15.608	38.497
E G5	Elshitsa	py	Stage I	18.495	15.608	38.498
E 33/99	Elshitsa	cp	Stage II	18.492	15.615	38.522
E 36/98	Elshitsa	cp	Stage II	18.518	15.613	38.518
BU10A	Elshitsa	cp	Stage II	18.534	15.632	38.615
E 500	Elshitsa	bn	Stage II	18.513	15.622	38.551
E 01/94	Elshitsa	sp-gn	Stage III	18.525	15.635	38.590
E 06/99	Elshitsa	gn	Stage III	18.494	15.610	38.514
BU10B	Elshitsa	gn	Stage III	18.505	15.620	38.543
VV 124/70	Vlaykov Vruh	py	Stage III	18.475	15.610	38.502
VV 125/70	Vlaykov Vruh	cp	Stage III	18.481	15.618	38.531
VV 17/99	Vlaykov Vruh	py	Stage IV	18.432	15.636	38.519
VV 24/99	Vlaykov Vruh	py	Stage V	18.531	15.637	38.621
R 10/97	Radka	py	Stage I	18.491	15.616	38.533
R 79/97	Radka	cp	Stage II	18.490	15.621	38.567
R 614	Radka	en	Stage II	18.488	15.619	38.537
R 201/93	Radka	sp-gn	Stage III	18.497	15.627	38.573
R 64/97	Radka	py	Stage IV	18.518	15.647	38.630

2σ error: $^{206}Pb/^{204}Pb$=0.013; $^{207}Pb/^{204}Pb$=0.016; $^{208}Pb/^{204}Pb$=0.054. Mineralisation stages are according to Figs. 6 and 9

py pyrite, *cp* chalcopyrite, *bn* bornite, *sp* sphalerite, *gn* galena, *en* enargite

body cut by epithermal veins in the southwestern part of the Elshitsa deposit (AvQ 032), one rhyodacite affected by quartz–sericite–pyrite alteration from the southwestern part of Elshitsa (AvQ 101), the Vlaykov Vruh granodiorite porphyry (AvQ 031), and one aplite–pegmatite dyke crosscutting the latter (AvQ 099). Dating the hydrothermal activity in the two neighboring deposits has been attempted with one sample of hydrothermal rutile from the Vlaykov Vruh deposit (VV 46/99) and two samples of hydrothermal rutile and anatase from the phyllic alteration zone of the Elshitsa–West deposit (E 63/99 and E 64/99; Fig. 2b).

Concordant ages have been obtained only for zircons from the Elshitsa granite and the Elshitsa subvolcanic dacite. Only air-abraded zircon grains yielded concordant dates, non-abraded zircons usually showing lead loss (Table 6). Four abraded grains from the Elshitsa granite, representing the plutonic part of the magmatic system, are concordant within analytical error and reveal an intrusive concordia age of 86.61±0.31 Ma (mean $^{206}Pb/^{238}U$ age of 86.62±0.02 Ma). The ε-Hf values for concordant zircons range from +6.2 to +7.9 (Table 7). The Elshitsa subvolcanic dacite shows an intrusive concordia age (based on three concordant grains, within analytical error) of 86.11± 0.27 Ma (mean $^{206}Pb/^{238}U$ age of 86.11±0.23 Ma) and ε-Hf values ranging from +7.2 to +9.6 (Table 7). Three of the analyzed zircons from this sample are significantly older suggesting the presence of an inherited component. Two of the discordant zircons define an upper intercept at 465±7 Ma, indicating an important assimilation of Paleozoic crustal material by the Late Cretaceous magmas. For convenience, only concordant zircons are plotted in Fig. 16. Because of the presence of inherited components in the zircons from the Elshitsa volcanic rocks, as well as from the Vlaykov Vruh granodiorite (Fig. 5a) and pegmatite (Fig. 5b), these three samples display discordant ages, not allowing us to determine precisely their crystallization age.

Among the three studied samples of hydrothermal Ti-oxides, only one sample of rutile from the high-temperature porphyry mineralization at Vlaykov Vruh (Fig. 5g) revealed a mean $^{206}Pb/^{238}U$ age of 85.6±0.9 Ma (Fig. 16c). The low-temperature TiO_2 varieties from the epithermal ore bodies at Elshitsa were not suitable for U–Pb analyses due to their very low U-content (< 5 ppm U) and hence very low radiogenic Pb addition.

Discussion

Origin of magmas in the southern part of the Panagyurishte district

At a district scale, the Elshitsa magmatic complex is the only one in which the deep plutonic, the subvolcanic, and the extrusive facies are preserved and exposed at the

Table 4 Rb, Sr, Sm, and Nd concentrations and isotopic compositions of whole rock samples from the southern part of the Panagyurishte district

Sample	Rock type	Rb (ppm)	Sr (ppm)	Rb/Sr	$^{87}Rb/^{86}Sr$	$^{87}Sr/^{86}Sr$	Error (±2SE)[a]	$^{87}Sr/^{86}Sr_i$ (t=85Ma)	Sm (ppm)	Nd (ppm)	Sm/Nd (ppm)	$^{147}Sm/^{144}Nd$	$^{143}Nd/^{144}Nd$	Error (±2SE)[a]	$^{143}Nd/^{144}Nd_i$ (t=85Ma)	ε_{Nd} (t=85Ma)
E 60/99	Two-mica gneiss	49	126	0.3896	1.0913	0.716704	9	0.71539								
E 17/00	Variscan granite	16	717	0.0227	0.0637	0.708537	7	0.70846								
E 18/00	Variscan granite	121	169	0.7171	2.0091	0.717985	12	0.71556								
E 19/00	Turonian marl	34	1139	0.0296	0.0829	0.707653	26	0.70755								
E 20/00	Andesite	5.8	550	0.0105	0.0295	0.705908	11	0.70587	4.4	21.6	0.2019	0.122108	0.512473	11	0.51241	−2.4
R 01/00	Andesite	65	503	0.1288	0.3603	0.705627	7	0.70519	4.0	19.6	0.2031	0.122838	0.512616	8	0.51255	0.4
E 53/99A	Andesite	22	159	0.1357	0.3796	0.706307	11	0.70585	3.8	17.5	0.2153	0.130223	0.512528	14	0.51246	−1.4
E 53/99B	Rhyodacite	73	241	0.3026	0.85	0.706618	10	0.70560	1.9	11.4	0.1672	0.101135	0.512514	23	0.51246	−1.4
R 17/99	Rhyodacite	81	80	1.0174	2.8477	0.709138	12	0.70570	1.7	11.0	0.1576	0.095324	0.512497	23	0.51244	−1.7
VV 35/99	Rhyodacite	67	408	0.1643	0.4599	0.706728	8	0.70617	2.2	13.3	0.1646	0.099540	0.512567	8	0.51251	−0.3
R 19/99	Rhyodacite	16	438	0.0372	0.1042	0.706068	7	0.70594	2.2	15.0	0.1453	0.087842	0.512508	5	0.51246	−1.4
VV 36/99	Subvolcanic rhyodacite	64	238	0.2685	0.75	0.707153	10	0.70625	2.5	14.7	0.1715	0.103734	0.512547	14	0.51249	−0.8
E 66/99	Subvolcanic rhyodacite	61	100	0.6055	1.6945	0.708129	8	0.70608	1.9	11.8	0.1628	0.098470	0.512575	27	0.51252	−0.2
E 16/97	Elshitsa granite	100	248	0.4016	1.1239	0.706123	8	0.70477	1.7	11.0	0.1552	0.093885	0.512558	9	0.51251	−0.4
E 17/94	Elshitsa granite	113	228	0.4966	1.3896	0.706365	9	0.70469								
VV 06/99	Vlaykov Vruh granodiorite	44	260	0.1692	0.4736	0.706325	12	0.70575								
VV 23/99	Vlaykov Vruh granodiorite	31	359	0.0871	0.2437	0.706094	9	0.70580	2.3	14.7	0.1565	0.094656	0.512498	6	0.51245	−1.6
R 16/99	Red marl	22	401	0.0539	0.1508	0.707844	9	0.70766								
R 15/99	Senonian flysch (marl)	18	436	0.0413	0.1155	0.707719	8	0.70758								

[a] −2 SE represents two standard errors on the least significant digits on the analytical mean, based on within-run statistics

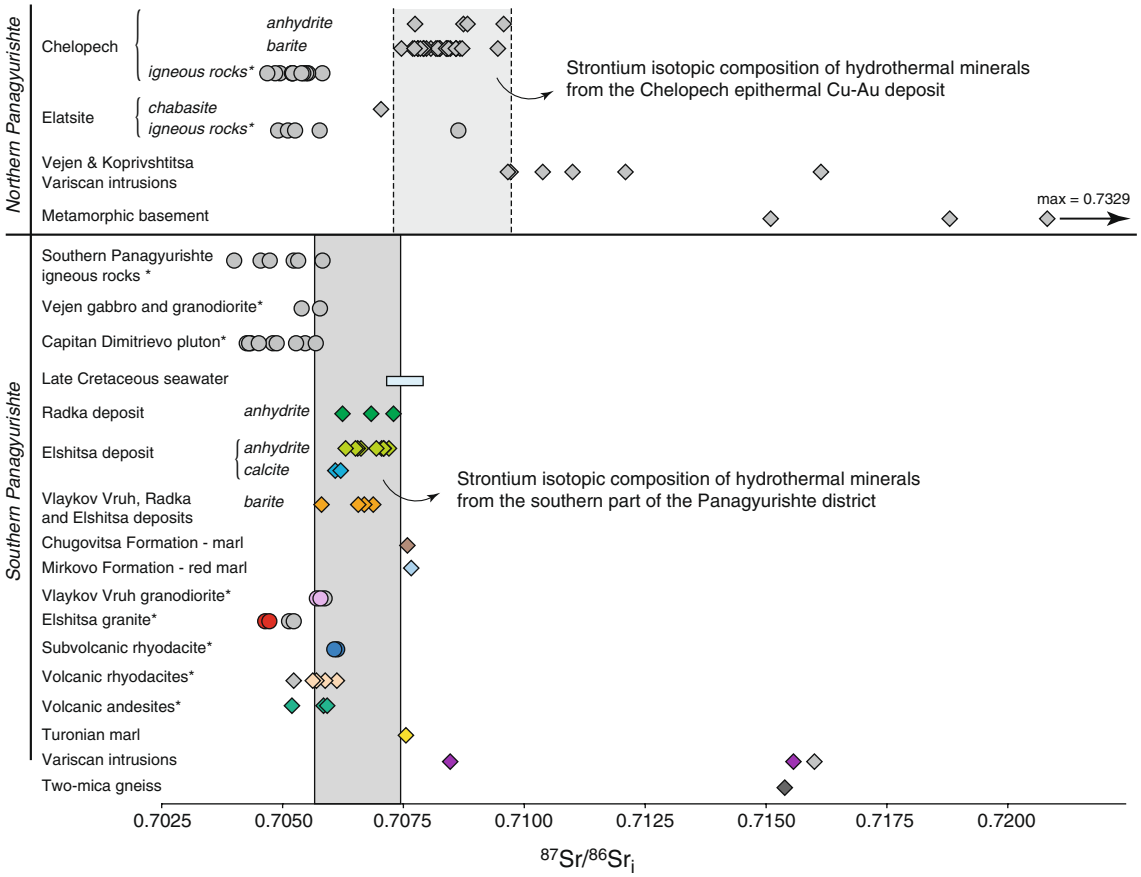

Fig. 13 Strontium isotope data for host rocks and hydrothermal minerals in southern and northern parts of the Panagyurishte district. Data from this study are presented in *color* and published data are presented as *light-gray symbols*. Late Cretaceous igneous rocks are marked with *asterisk*. The sources for the published data are: Chelopech hydrothermal minerals (Moritz et al. 2001, 2003; Jacquat 2003); Chelopech igneous rocks (Stoykov et al. 2003, 2004); Elatsite hydrothermal minerals and igneous rocks (von Quadt et al. 2002, 2005); Vejen and Koprivshtitsa Variscan intrusions in Northern Panagyurishte (Kamenov et al. 2002; von Quadt et al. 2002, 2005; Jacquat 2003); metamorphic basement in Northern Panagyurishte (Jacquat 2003); Southern Panagyurishte Late Cretaceous igneous rocks from various magmatic centers (von Quadt et al. 2005); Capitan Dimitrievo pluton in the southernmost part of the district (Kamenov et al. 2003b; von Quadt et al. 2005); Late Cretaceous seawater (Koepnick et al. 1985); few data for the Elshitsa granite, subvolcanic rhyodacites, and the Lesitchevo Variscan intrusion from Southern Panagyurishte (Peytcheva et al. 2003) are plotted as well. Data for the Northern Panagyurishte are corrected for 90 Ma, and data for the Southern Panagyurishte—for 85 Ma

present-day surface. For this reason, several porphyry–epithermal pairs have been described here, mainly hosted by the Elshitsa and Radka volcanic strips, preserved along the SW and NE margins of the Elshitsa pluton, respectively. The Elshitsa magmatic complex shares geochemical characteristics with typical subduction-related magmatic series defined in other parts of the ABTS belt, such as the Eastern Srednogorie (Boccaletti et al. 1974, 1978; Stanisheva-Vassileva 1980), the Timok zone in Serbia (Karamata et al. 1997; von Quadt et al. 2003), and the Banat zone in Romania (Berza et al. 1998; Dupont et al. 2002). The petrological and geochemical data reported in this paper suggest existence of continuous medium- to high-K, calc-alkaline magmatic series in the Elshitsa magmatic complex. The radiogenic isotope geochemical data presented in the previous sections provide fundamental constraints on the petrogenesis of the Elshitsa suite.

Many lines of evidence suggest a major role of fractional crystallization in the evolution of magmas in the southern Panagyurishte district. These include: (1) the close spatial and probably temporal association of the eruptive products of the lower andesitic and the upper dacitic volcanic units; (2) the increase of alkalis, LILE and HFSE, and the decrease of TiO_2, FeO*, and MgO with increasing SiO_2 (Figs. 10 and 11); (3) variations of incompatible trace elements with trends from low abundances in andesites to higher abundances in dacites and rhyodacites and the felsic subvolcanic rocks; and (4) overall increase of total REE

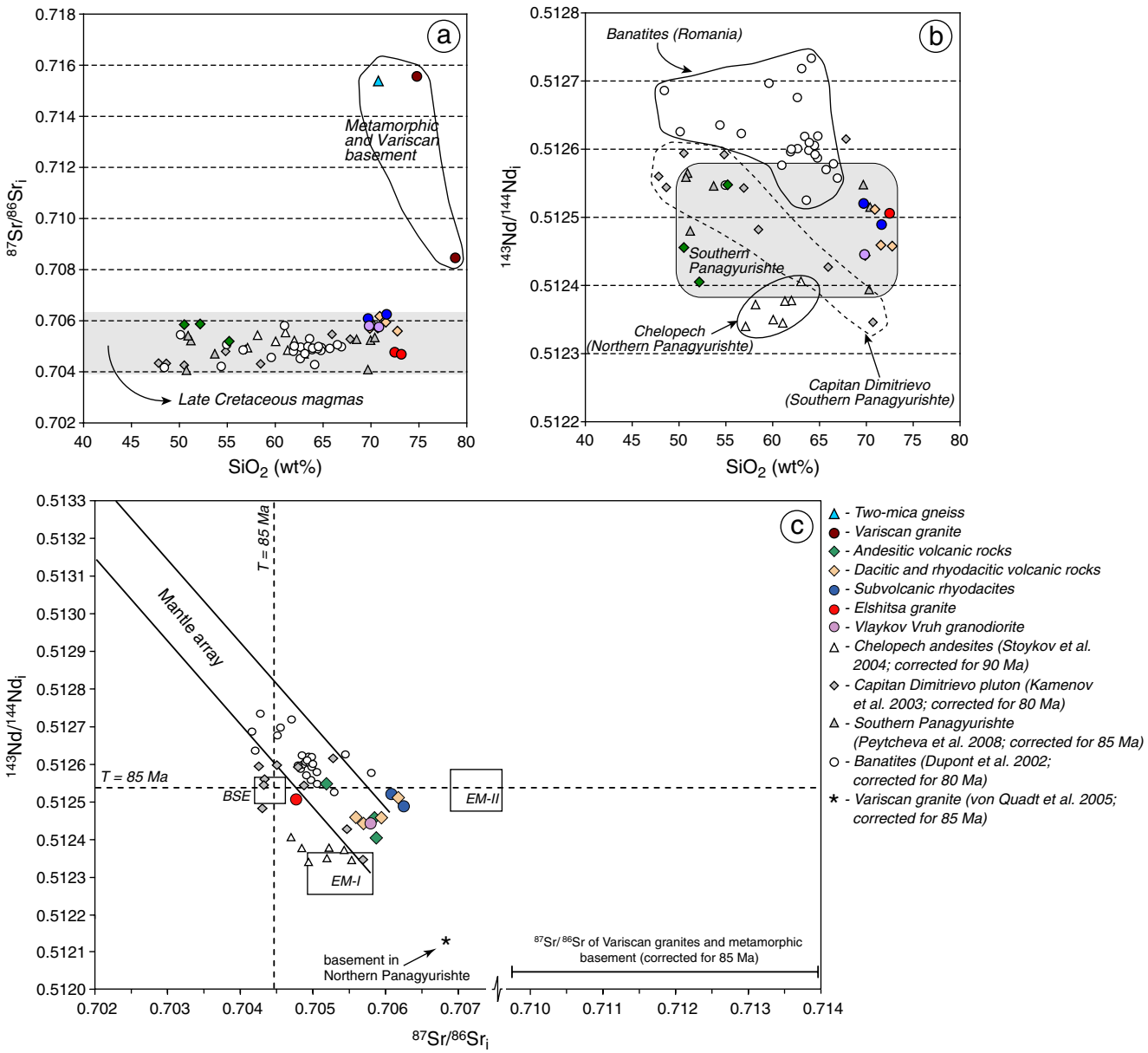

Fig. 14 **a** SiO_2 versus $(^{87}Sr/^{86}Sr)_i$; **b** SiO_2 versus $(^{143}Nd/^{144}Nd)_i$; and **c** $(^{87}Sr/^{86}Sr)_i$ versus $(^{143}Nd/^{144}Nd)_i$ diagrams for rocks from the Southern Panagyurishte district. Fields of the EM1 and 2 (enriched mantle 1 and 2) and BSE (bulk silicate earth) are given (corrected for 85 Ma) according to Zindler and Hart (1986) and Hart and Zindler (1989). *Dashed lines* correspond to the Sr and Nd isotope values of the undifferentiated reservoir, corrected for 85 Ma

contents with increasing SiO_2 (Fig. 10e). Most probably fractionation of olivine, hornblende, Ti-bearing magnetite, apatite, clinopyroxene, zircon, and possibly K-feldspar has played an important role in the process of magmatic crystallization at Elshitsa. The general absence of Eu anomalies suggests a reduced fractionation of plagioclase.

The occurrence of cognate gabbroic inclusions and lenses in the most evolved rocks (granodiorite to granites) in the western parts of the Elshitsa pluton (Boyadjiev and Chipchakova 1962; Dabovski 1963) indicates that fractional crystallization was accompanied to some extent by magma mixing and mingling at various stages of differentiation, as suggested by Ivanov et al. (2002) and Peytcheva et al. (2008) for the Boshulia pluton, located south of the Elshitsa magmatic complex.

The geochemical and isotopic variations in the Elshitsa magmatic complex also suggest involvement of various crustal components in the evolution of the magmatic series. In fact, many of the isotopic signatures of the felsic magmas seem to favor a model involving contamination

Table 5 Sr concentrations and isotopic compositions of hydrothermal calcite, barite and anhydrite from the Elshitsa, Radka and Vlaykov Vruh deposits

Sample	Deposit	Mineral	Mineralisation stage	Sr (ppm)	$^{87}Sr/^{86}Sr$	Error (±2SE)[a]
E 46/98	Elshitsa	Calcite	Stage III	642	0.706115	7
E 39/99	Elshitsa	Calcite	Stage III	622	0.706165	13
E 50/97	Elshitsa	Barite	Stage III	1,076	0.706691	8
E MPI404	Elshitsa	Barite	Stage III	1,689	0.706874	6
R 506	Radka	Barite	Stage III	1,252	0.706565	7
VV 39/99	Vlaykov Vruh	Barite	Stage IV	1,582	0.705805	10
R 561	Radka	Anhydrite	Stage V	1,273	0.706835	8
R 570/67	Radka	Anhydrite	Stage V	1,640	0.707295	12
R 29/98	Radka	Anhydrite	Stage V	1,298	0.706241	6
E 32/1967	Elshitsa	Anhydrite	Stage V	1,131	0.706581	7
E 49/97	Elshitsa	Anhydrite	Stage V	1,063	0.706510	6
E V1	Elshitsa	Anhydrite	Stage V	1,078	0.706554	8
E 13/98	Elshitsa	Anhydrite	Stage V	1,456	0.707201	9
E 17/98	Elshitsa	Anhydrite	Stage V	945	0.707050	7
E 22/98	Elshitsa	Anhydrite	Stage V	1,002	0.706305	7
E 04/89	Elshitsa	Anhydrite	Stage V	1,207	0.707093	10
E 79/99	Elshitsa	Anhydrite	Stage V	1,300	0.707087	8
E 40/98	Elshitsa	Gypsum	Stage V	593	0.706940	6

[a] −2 SE represents two standard errors on the least significant digits on the analytical mean, based on within-run statistics

of mantle-derived magmas during ascent through the continental crust. These include: (1) occurrence of pre-Mesozoic basement xenoliths in the subvolcanic intrusions and dykes, as well as in the periphery of the Elshitsa pluton (Boyadjiev and Chipchakova 1962, 1965; Dabovski 1963); (2) systematic inherited basement components in the magmatic zircons from dacites and rhyodacites and the subvolcanic felsic varieties; (3) the two samples from the Elshitsa granite show the strongest mantellic Sr isotopic signatures among the analyzed suite of magmatic rocks, indicating that at deeper level (magma chamber), the contamination process was less pronounced, than in the subvolcanic and extrusive facies in which the magmas traveled across additional 3 to 4 km upper crust until they reached the site of crystallization; (4) combination of Nd and Sr isotope characteristics of the Elshitsa magmas explicitly indicates mixed crustal–mantle signatures similar to the Capitan Dimitrievo pluton and other Late Cretaceous magmatic rocks from the Banat area in Romania in the northern sector of the ABTS belt (Fig. 14c); and (5) ε-Hf values of +6.2 to +8.9 of magmatic zircons from the felsic intrusions and subvolcanic bodies also support a mixed crustal–mantle origin for the magmas at Elshitsa.

The Pb isotope data are more equivocal. In general, the southern Panagyurishte magmas show large variations in the $^{206}Pb/^{204}Pb$ ratio with only minor variations in $^{207}Pb/^{204}Pb$ and $^{208}Pb/^{204}Pb$ (Fig. 12). These Pb isotope signatures seem to be a general feature of the Central Srednogorie arc magmatism as a whole and cannot be explained by a single model of assimilation of the Variscan basement. In Fig. 12, the Elshitsa suite samples form a nearly linear array, which most probably reflects mixing of two isotopically distinct components in terms of $^{206}Pb/^{204}Pb$ and similar or very close $^{207}Pb/^{204}Pb$ and $^{208}Pb/^{204}Pb$ ratios; however, the limited database for the Pb isotopic compositions of the Balkanide-type metamorphic complex and the Variscan granitoids do not allow correct quantification. In Fig. 12, fields for gneisses and Variscan intrusions from the Central Srednogorie (data from Amov et al. 1973, 1982) are not age-corrected for 85 Ma because the published Pb isotope data have no concentration values, and thus, the basement lithologies are difficult to define as potential mixing end-members. Alternatively, the existing data could be tentatively interpreted as a result of: (1) large-scale mantle source heterogeneities, given also the evidence that on the $^{87}Sr/^{86}Sr_{(i)}$ versus $^{143}Nd/^{144}Nd_{(i)}$ diagram, the Chelopech and the southern Panagyurishte magmatic rocks plot along a trend between EM-I and EM-II (Fig. 14c) and/or (2) assimilation by the parental mantellic magmas of dominantly upper continental crust material in the Southern Panagyurishte and of lower continental crust material in the

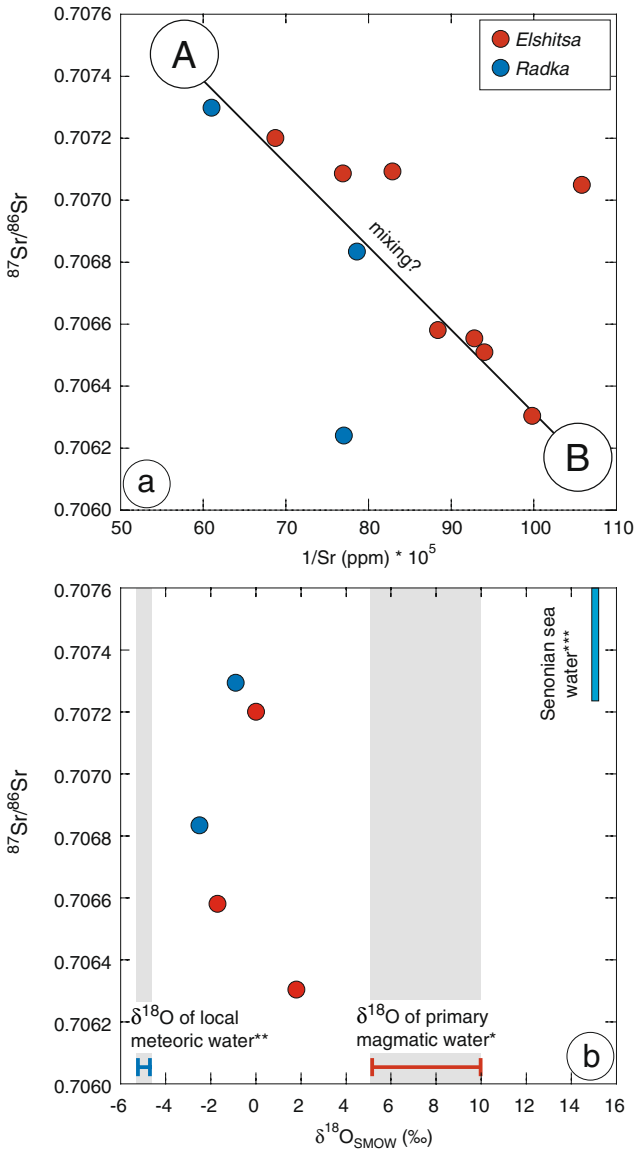

Fig. 15 Strontium isotope data for hydrothermal anhydrite from Elshitsa and Radka epithermal deposits. **a** $^{87}Sr/^{86}Sr$ versus 1/Sr (ppm) $*10^5$ diagram. The observed negative correlation is interpreted in terms of fluid mixing between two hypothetical end-member fluids—*A* and *B* (for discussion, see text); **b** Oxygen and strontium isotopic compositions of the hydrothermal fluid that precipitated anhydrite at Elshitsa and Radka. Oxygen isotopic composition of primary magmatic water (Taylor 1974) and Late Cretaceous local meteoric water (Kouzmanov et al. 2003), as well as strontium and oxygen isotopic compositions of Late Cretaceous seawater (Koepnick et al. 1985; Claypool et al. 1980) are indicated for comparison

northern part (Chelopech), possibly due to different depth of magma chamber formation.

In a regional context, some particularities of the Late Cretaceous magmas from different parts of the ABTS belt can be inferred: (1) the available Sr–Nd isotopic data set for primitive magmas is very restricted—most of the published data is for relatively evolved compositions, thus making very difficult correct interpretation of the source effect; (2) banatites from South Romania (Dupont et al. 2002) have isotopically the most primitive compositions in the ABTS belt (generally higher $^{143}Nd/^{144}Nd_{(i)}$ and lower or partially overlapping $^{87}Sr/^{86}Sr_{(i)}$ compositions than the Late Cretaceous magmas in Central Srednogorie). Several scenarios are possible to explain such a difference: inhomogeneity of the metasomatized mantle edge along the subduction front during the Late Cretaceous; different thickness of the crust and/or assimilation of different middle–upper crustal material in different parts of the arc; (3) Southern Panagyurishte magmas display more primitive compositions compared to Chelopech in the Northern Panagyurishte, due to a difference in the magma source or a different nature of the assimilated pre-Mesozoic basement (Balkanide-type high-grade metamorphic rocks in the south versus low-grade Diabase–Phyllitoid complex in the north; see above).

Origin of porphyry and epithermal deposits in the southern Panagyurishte district

In the southern Panagyurishte district, porphyry Cu and epithermal Cu–Au deposits are genetically and spatially related to the subvolcanic NW-trending intrusions and dykes, cropping out in the volcanic strips on both sides of the Elshitsa pluton (Fig. 2a). Both deposit types are structurally controlled and were formed along WNW-trending steeply dipping diagonal faults (N110-120). Mineralization processes and stable isotopic signatures in both systems show many similarities, favoring the interpretation of a common origin of mineralizing fluids and ore metals and a very probable close time relationship.

One of the still debated questions in the porphyry–epithermal models is the timing of ore formation in the porphyry and epithermal environment in complex magmatic–hydrothermal systems. A few case studies (e.g. Far Southeast-Lepanto, Philippines: Arribas et al. 1995; Hedenquist et al. 1998; Maricunga belt, northern Chile: Muntean and Einaudi 2001) tried to elucidate this question, reporting almost synchronous (≤100,000 years) to clearly separate in time (as much as 900,000 years) porphyry and high-sulfidation ore formation in which the porphyry fluid and alteration–mineralization is reported to be directly related to the spatially associated epithermal ore bodies.

In this contribution, we attempted to date the timing of magmatic and hydrothermal processes using high-precision U–Pb dating in the case of Vlaykov Vruh porphyry and Elshitsa epithermal pair. Unfortunately, only a few samples were suitable for correct dating, and only the timing of porphyry ore formation at Vlaykov Vruh was determined with an age of 85.6±0.9 Ma, immediately following or

Table 6 U–Pb zircon isotope data for the Elshitsa granite and Elshitsa subvolcanic rhyodacite, and rutile data from the Vlaykov Vruh deposit

Number	Meas. *N*°	Size fraction (μm)	Weight (mg)	Description	U (ppm)	Pb (ppm)	$^{206}Pb/^{204}Pb$	$^{206}Pb/^{238}U$	2σ	$^{207}Pb/^{235}U$	2σ	$^{207}Pb/^{206}Pb$	2σ	$^{206}Pb/^{238}U$ apparent age	Rho
AvQ 029 (magmatic zircon–Elshitsa granite)															
1	IP29	75–100	0.0033	Isometric	121	3.74	70.3	0.01348	0.00008	0.089	0.005	0.048	0.002	86.28	0.52
2	IP33	75–100	0.0109	Prism abr Pale beige	103	2.28	154.8	0.01356	0.00008	0.089	0.005	0.0477	0.0002	86.84	0.55
3	IP86	75–100	0.0080	Prism abr Pale beige	62.7	1.15	284.1	0.01352	0.00015	0.090	0.002	0.0482	0.0011	86.59	0.52
4	IP87	75–100	0.0020	Prism abr Pale beige	163	3.20	206.8	0.01355	0.00014	0.090	0.003	0.0483	0.0015	86.78	0.42
5	IP89[a]	75–100	0.0033	Prism Pale beige	189	3.61	215.1	0.01316	0.00008	0.089	0.004	0.049	0.002	84.30	0.51
6	IP90[a]	75–100	0.0051	Prism Pale beige	167	2.87	415.6	0.01318	0.00007	0.088	0.002	0.0484	0.0009	84.40	0.43
AvQ 032 (magmatic zircon–Elshitsa subvolcanic rhyodacite)															
7	IP175	75–100	0.0102	3 Long prism Beige, abr	114	1.90	559.6	0.01348	0.00006	0.0891	0.0008	0.0479	0.0003	86.32	0.62
8	IP176	75–100	0.0103	4 Long prism Beige, abr	97.2	1.62	542.8	0.01342	0.00006	0.0892	0.0009	0.0485	0.0003	85.91	0.66
9	IP177	75–100	0.0154	4 Long prism Beige, abr	99.1	1.78	356.0	0.01346	0.00008	0.089	0.002	0.0481	0.0012	86.16	0.43
10	IP103[a]	75–100	0.0045	Long prism Beige	118	2.89	107.4	0.01316	0.00008	0.089	0.006	0.049	0.004	84.31	0.62
11	IP104[a]	75-100	0.0090	Long prism Beige	118	2.56	133.0	0.01256	0.00008	0.082	0.005	0.048	0.003	80.43	0.56
12	IP105[b]	75–100	0.0120	Isometric Water clear	94.2	9.57	1969.8	0.09653	0.00060	0.991	0.010	0.0744	0.0006	594.1	0.64
13	2573[b]	63–125	0.0085	Prism Transp	80.0	1.54	374.6	0.01375	0.00010	0.139	0.003	0.0733	0.0011	88.01	0.55
14	2574[b]	63–125	0.0049	Prism Transp	318	21.80	1181.8	0.06833	0.00034	0.529	0.003	0.0561	0.0001	426.1	0.89
15	2575[a]	63–125	0.0058	Prism Transp	137	3.57	87.8	0.01207	0.00015	0.081	0.005	0.049	0.003	77.32	0.42
VV 46/99 (hydrothermal rutile–Vlaykov Vruh porphyry Cu deposit)															
16	2564	125–250	0.0101		31.1	1.09	55.0	0.01337	0.00016	0.091	0.005	0.049	0.002	85.59	0.49
17	2565	125–250	0.0100		28.7	0.64	97.1	0.01339	0.00028	0.084	0.004	0.0456	0.0009	85.72	0.52

Errors (%): 2σ—for the two zircon samples (AvQ 029 and AvQ 032) and 1σ—for the rutile sample (VV 46/99)

abr. abraded, *prism.* prismatic, *transp.* transparent, *Rho* correlation coefficient $^{206}Pb/^{238}U$–$^{207}Pb/^{235}U$

[a] Sample with lead loss

[b] Zircons with inherited core

Table 7 Hf isotope data for zircons from the Elshitsa granite and Elshitsa subvolcanic rhyodacite (numbers are as in Table 6)

Number	Meas. *N*°	$^{176}Hf/^{177}Hf$	2s error	ε Hf today	ε Hf (*t*=85Ma)
AvQ-029 (Elshitsa granite)					
1	IP33	0.282901	0.000006	4.6	6.2
2	IP86	0.282951	0.000002	6.3	7.9
3	IP87	0.282912	0.000011	5.0	6.6
4	IP90[a]	0.282917	0.000006	5.1	6.7
AvQ-032 (Elshitsa subvolcanic rhyodacite)					
5	IP175	0.282947	0.000007	6.2	7.8
6	IP176	0.282977	0.000019	7.2	8.9
7	IP177	0.282929	0.000004	5.6	7.2
8	IP104[a]	0.282983	0.000005	7.5	9.1
9	IP105[b]	0.281937	0.000004	−30	−28
10	2575[a]	0.282997	0.000009	8.0	9.6

[a] Sample with lead loss

[b] Zircon with inherited core

partially overlapping within analytical error the crystallization of the subvolcanic dacitic bodies at Elshitsa dated at 86.11±0.23 Ma (mean $^{206}Pb/^{238}U$ age). The Elshitsa granite, representing the deeper magma chamber level of this magmatic complex yielded the oldest age with 86.62± 0.02 Ma (mean $^{206}Pb/^{238}U$ age), but also overlapping within analytical error with the subvolcanic bodies. The timing of epithermal ore formation at Elshitsa still remains uncertain. However, we believe that it was directly related to the porphyry ore formation at Vlaykov Vruh based on: (1) field evidence indicating a gradual transition between the Vlaykov Vruh granodiorite and the subvolcanic dacite and rhyodacite dykes at Elshitsa; (2) the observed lateral outward zonation from high- to lower-temperature alteration mineral assemblages from the porphyry Cu system at Vlaykov Vruh toward the Elshitsa–West sector of the epithermal system (Kouzmanov 2001); and (3) the almost identical sulfur and oxygen isotopic compositions of hydrothermal minerals in both systems, with a characteristic decrease of $\delta^{34}S$ values through time, attributed to progressive oxidation of the fluids and sulfur isotope fractionation due to hydrolysis of magmatic SO_2 (Kouzmanov et al. 2003).

Lead isotopic compositions of sulfides from the studied porphyry and epithermal deposits have very similar values (Fig. 12c and d). This reveals that both deposit types belong to the same metallogenic event and have a similar source of Pb and most probably of the other metals. As the ore samples from Vlaykov Vruh, Elshitsa, and Radka deposits plot exactly in the middle of the trend defined by the Late Cretaceous magmatic rocks on the Pb isotope diagrams (Fig. 12a and b), the most plausible interpretation is that Pb is of magmatic origin and that it was directly released by the ore-related Late Cretaceous magmas. The lead isotopic signature of fine-grained pyrite from the early massive pyrite bodies at Elshitsa and from "ore clasts" have identical compositions as the younger copper and polymetallic ores, thus supporting the common epithermal origin of the mineralization at Elshitsa as a whole and contradicts the two-stage model proposed earlier by Bogdanov (1984).

The Sr isotopic compositions of hydrothermal minerals from the epithermal Cu–Au deposits fall between the Sr isotope ratios of Upper Cretaceous magmatic rocks and the more radiogenic basement rocks (Fig. 13). From a genetic point of view, the rhyodacitic volcanic and subvolcanic rocks are the most likely source of Sr for the epithermal mineralization, since they are the major host rocks. The more radiogenic composition of hydrothermal minerals with respect to the host felsic rocks shows that there was an additional Sr source. Figure 15a suggests an extensive circulation of the hydrothermal fluids through basement lithologies, such as metamorphic rocks and Variscan granitoids with radiogenic Sr, in addition to the Late Cretaceous magmatic source of Sr. Strontium and oxygen isotopic compositions of hydrothermal anhydrites from the Radka and Elshitsa deposits (Fig. 15b) allow us to exclude Late Cretaceous seawater as a potential source of external fluids involved in the magmatic–hydrothermal system.

The geochemical features, alteration, ore mineralogy, and paragenesis, including lateral and vertical zonations in the Elshitsa epithermal Cu–Au deposit, described above, allows us to attribute the deposit to the deep part of a high-sulfidation epithermal system, according to the terminology of Hedenquist et al. (2000) and Sillitoe and Hedenquist (2003), genetically related to the adjacent Vlaykov Vruh porphyry Cu system. Local overprint of early stage typical high-sulfidation to very high-sulfidation mineral assemblage (in the sense of Einaudi et al. 2003) consisting of pyrite ± enargite ± covellite ± goldfieldite ± alunite and illite by intermediate-sulfidation assemblages (with characteristic Cu–Bi–Te–Pb–Zn signatures) constituting the

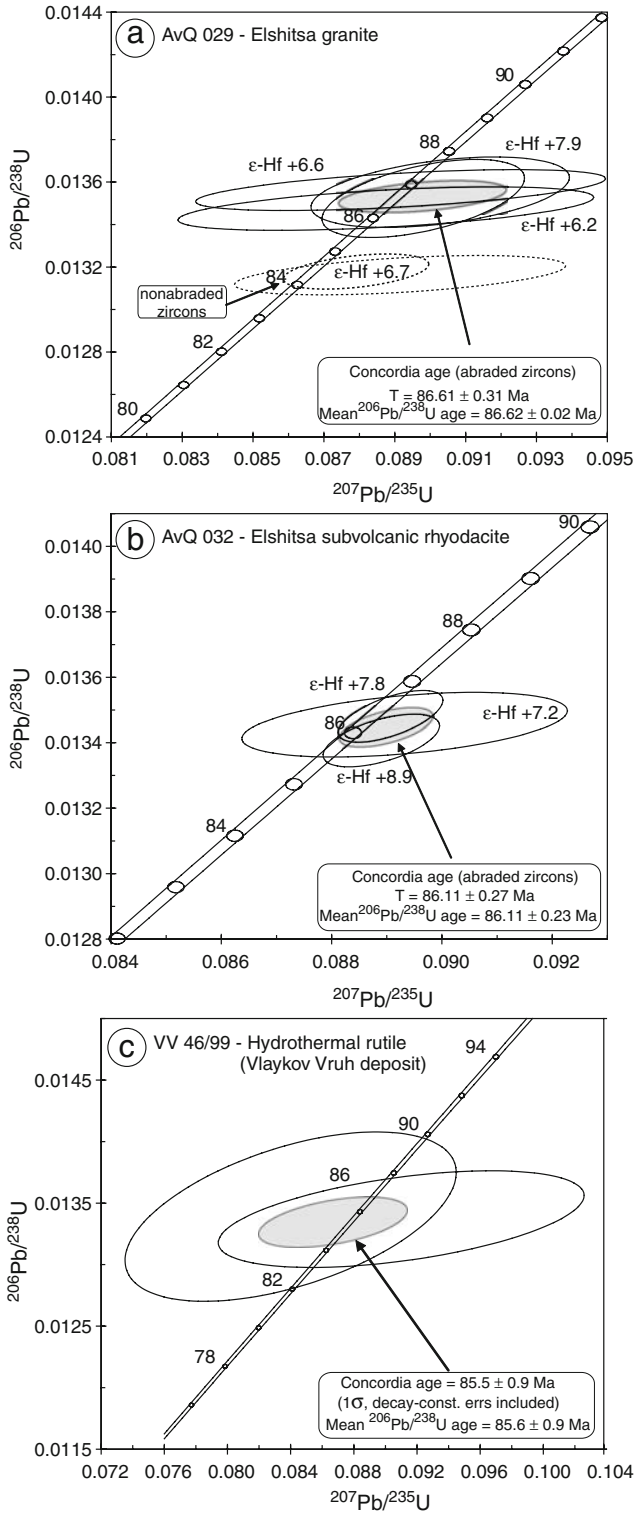

Fig. 16 U-Pb concordia diagrams of the Elshitsa granite AvQ 029 (**a**), the Elshitsa subvolcanic rhyodacite AvQ 032 (**b**), and the hydrothermal rutile from Vlaykov Vruh deposit VV 46/99 (**c**). Individual analyses are shown as 2σ error ellipses for zircons and 1σ ellipses for rutile. Given ages are weighted mean $^{209}Pb/^{238}U$ ages at 95% confidence level. Numbers correspond to the zircon numbers from Table 6. Only concordant zircons, not showing Pb loss or inheritance, are presented on the plots (see text for explanation). Measured ε-Hf values for single zircons are indicated as well

main economic mineralization at Elshitsa is observed. The latter telescoping feature is probably a common characteristic of high-sulfidation systems, no matter if they are hosted by magmatic or carbonate rocks, as described by Jannas et al. (1999) for the El Indio deposit in Chile, Baumgartner et al. (2008) for the Cerro de Pasco polymetallic deposit in Peru, and Bendezú (2007) for the Colquijirca district in Peru.

Southern versus northern Panagyurishte Late Cretaceous magmas and ore deposits

Progressive younging of the magmatism from ~92 Ma in the north (in the area of Elatsite–Chelopech) to ~78 Ma in the south (Capitan Dimitrievo) correlates with a north-to-south geochemical trend of decreasing crustal input into the mantle-derived magmas (von Quadt et al. 2005) and is generally interpreted as a direct consequence of slab roll-back or hinge slab retreat during oblique subduction (Neubauer 2002; Lips 2002; Handler et al. 2004; Moritz et al. 2004; von Quadt et al. 2005; Kamenov et al. 2007).

The northern part of the Panagyurishte district hosts the largest porphyry Cu and epithermal Cu–Au deposits, compared to the southern part where only relatively small deposits were formed (Table 1). The most illustrative example for such N–S trend is given by the Pb isotope signatures of sulfide minerals from northern and southern deposits in the district (Fig. 12c and d), showing an almost linear tendency with increasing radiogenic compositions toward the north. Similar arguments are given by von Quadt et al. (2005) using ε-Nd and ε-Hf compositions of Late Cretaceous magmatic rocks. In contrast, the Sr isotopic compositions of magmas in the northern and southern parts of the district remain surprisingly identical (Fig. 14a). However, the hydrothermal sulfates at Chelopech show higher $^{87}Sr/^{86}Sr$ ratios compared to the Radka and Elshitsa sulfates and carbonates (Fig. 13), revealing a more intense interaction of the ore-forming fluids with radiogenic metamorphic basement rocks and their detrital sedimentary products. Similarly, the more radiogenic Pb isotopic signatures of sulfides from ore deposits in the Northern Panagyurishte, compared to the southern part of the district (Fig. 12c), indicate more intense and extensive basement leaching at Elatsite and Chelopech than at Elshitsa and Vlaykov Vruh.

Besides the proposed slab retreat during subduction, an additional parameter that could have influenced the differences in magma chemistry is the thickness of the crust. The crustal thickness in the Panagyurishte corridor progressively decreases from the northernmost part (Elatsite–Chelopech area) to the area of the Elshitsa magmatic complex and then increases again toward the southernmost part of the transect (Capitan Dimitrievo; Fig. 1b). This variation of the crustal thickness changes in parallel with the crustal–mantle signature of the magmas, with an increasing mantle component from Elatsite southward down to the Elshitsa magmatic complex and the southerly adjacent Boshulia pluton both showing the strongest mantellic signatures (Peytcheva et al. 2008 and this study) and then again progressively decreasing southward to the Capitan Dimitrievo pluton (Kamenov et al. 2003b). The deeper erosional level in the southernmost part of the district, lacking economic mineralization for this reason, has probably additionally reduced the crustal thickness in the area.

Conclusions

The studied Vlaykov Vruh and Elshitsa deposits are the best example of tight spatial association of porphyry Cu and high-sulfidation epithermal Cu–Au systems within the richly mineralized Late Cretaceous Panagyurishte ore district, Central Srednogorie. The southern part of the Panagyurishte magmato-tectonic corridor, where the studied deposits are located, displays some geochemical and metallogenic particularities compared to the central and northern parts, hosting the largest mineralized systems.

The medium- to high-K calc-alkaline magmas of the Elshitsa magmatic complex, with a well pronounced mantle geochemical signature, are the most probable sources for metals and mineralizing fluids involved in the formation of Vlaykov Vruh porphyry Cu and Elshitsa epithermal Cu–Au deposits. Magma generation and evolution resulted from various processes such as fractional crystallization, crustal assimilation, and contamination, as well as magma mixing at different sites during the ascent of mantle-derived magmas across the crust. Strontium isotope evidence suggests large-scale interaction between mineralizing fluids and basement lithologies at Vlaykov Vruh–Elshitsa. Lead isotope compositions of hydrothermal sulfides allow discrimination of the porphyry and epithermal deposits in the Southern Panagyurishte district as a product of one single metallogenic event with a common source of metals. All field evidence and prevailing mineralogical and geochemical data indicate an epigenetic epithermal character of the mineralization in the different ore bodies at Elshitsa, excluding the scenario of two-stage massive sulfide–epithermal ore formation proposed in the past. At Elshitsa, an early stage high-sulfidation mineral assemblage was overprinted by intermediate-sulfidation paragenesis forming the main economic parts of the ore bodies.

Based on their common geological and structural setting, the ore-mineralogy and paragenesis, as well as their alteration and geochemical zonation, the Elshitsa and Vlaykov Vruh deposits are interpreted as the deep part of a high-sulfidation epithermal system and its spatially and genetically related porphyry Cu counterpart, respectively.

Acknowledgments This study was supported by the SCOPES Joint Research Project 7BUPJ62276.00/1, Swiss National Science Foundation grants 21-59041.99 and 200020-101853, and fellowship from the University of Geneva and grant for visit from the GEODE program for KK. R. Petrunov, P. Ignatovski, L. Naftali, I. Velinov, I. Chambefort, P. Marchev, S. Stoykov, S. Strashimirov, V. Jelev, and M. Ovtcharova are gratefully acknowledged for discussions. The authors would like to thank F. Capponi (University of Geneva)—for XRF analyses, M. Falchéri (University of Geneva)—for helping with the radiogenic isotope geochemistry, and P. Benoist-Julliot (ISTO-CNRS, Orléans)—for atomic absorption analyses of Sr. The journal reviewers Robert Frei and Volker Lüders are thanked for constructive comments, which improved the manuscript, and Bernd Lehmann is thanked for efficient editorial handling. This is a contribution to the ABCD-GEODE research program supported by the European Science Foundation.

Appendix 1—Analytical techniques

Whole-rock major oxides were analyzed by X-ray fluorescence spectrometry on powdered samples fused with $Li_2B_4O_7$ on a Philips PW2400 spectrometer with Rh anode at the "Centre d'Analyses Minérales," University of Lausanne, Switzerland. Trace elements and Rare Earth elements (REE) were analyzed by laser-ablation inductively coupled plasma-mass spectrometry (ICP-MS) on the same pellets at ETH—Zurich, Switzerland, applying the methodology described in Günther et al. (2001). Analytical results for major, REE and trace elements are presented in the Appendix 2.

Lead isotope analyses on whole-rocks were carried out at ETH—Zurich, Switzerland. Samples of about 50 mg of finely ground whole rock were washed in 3 N HNO_3 at 80 °C for 30 min. The residues were digested in 10-ml PFA-Teflon beakers with a mixture of 2 ml HF (21 N) and 4 ml HNO_3 (7.5 N) at 160 °C. After 5 days, the samples were dried and transferred to a nitrate form. Lead was separated by Sr Resin® (Eichrom, 50–100 μm) in 100-μl columns. The total procedure blank for lead was better than 10 pg. Pb was loaded on outgassed Re-filaments using the silica gel technique and measured on a MAT Finnigan 262 mass

spectrometer in static mode. The fractionation for lead was based on repeated measurements of the SRM982 standard. The fractionation factor was 0.095% per atomic mass unit. The analytical errors (2σ) were 0.03% for $^{206}Pb/^{204}Pb$, 0.04 % for $^{207}Pb/^{204}Pb$, and 0.08 % for $^{208}Pb/^{204}Pb$.

Lead isotope analyses on separates of chalcopyrite, pyrite, galena, bornite, enargite, and sphalerite–galena mixtures were carried out at the Department of Mineralogy, University of Geneva, Switzerland. Samples of 50 mg of ore minerals (except for galena—10 μg) were digested in sealed 20-ml Teflon beakers with a mixture of 3 ml 7 M HCl and 1 ml concentrated HNO_3 at 180°C. After conversion of the samples to bromide form, lead was separated by ion exchange chromatography. Procedural blanks were less than 120 pg Pb. Fractions of the purified lead were loaded on Re-filaments using the silica gel technique, and lead isotope ratios were measured on a MAT Finnigan 262 thermal ionization mass spectrometer in static mode. Lead isotope ratios were corrected for fractionation by a +0.10% atomic mass unit correction factor based on repeated analyses of the SRM981 international standard. The analytical errors (2σ) were 0.07% for $^{206}Pb/^{204}Pb$, 0.10% for the $^{207}Pb/^{204}Pb$, and 0.14% for the $^{208}Pb/^{204}Pb$.

Strontium and neodymium isotope analyses on whole-rock samples were conducted at the Department of Mineralogy, University of Geneva, Switzerland. About 200 mg of finely ground rock were digested with concentrated HF/HNO_3 in stainless steel bomb with Teflon liners. All solutions were evaporated, and the dry residues were dissolved in 2.5 N HCl, followed by Sr and Nd separation in ion exchange columns. Strontium and neodymium isotope analyses were performed on a seven-collector MAT Finnigan 262 thermal ionization mass spectrometer with extended geometry and stigmatic focusing using double Re-filaments. Strontium isotopic analysis was conducted in a semidynamic mode (triple collectors, measurement in jumping mode). The Sr isotope ratios were mass fractionation corrected to $^{88}Sr/^{86}Sr=8.375209$ and normalized to the Eimer and Amend® $SrCO_3$ standard, with $^{87}Sr/^{86}Sr=0.708000$ using an average of $0.708028\pm5\times10^{-6}$ (2SE; $n=52$) measured during the period of analyses. $^{143}Nd/^{144}Nd$ was measured in a semidynamic mode (quadruple collectors, measurement in jumping mode), mass fraction corrected to $^{146}Nd/^{144}Nd=0.721903$, and normalized to the La Jolla standard=0.511835. An average of $0.511838\pm6\times10^{-6}$ (2SE; $n=28$) was measured during the analyses.

For strontium isotope analyses of hydrothermal minerals, approximately 100 mg of finely ground anhydrite, barite, and calcite have been used. Barite and anhydrite were leached overnight in 6 N HCl at 110°C, and calcite samples were dissolved in 1.5 N HCl for 20 min. After evaporation of the solutions, the dry residues were dissolved in 2.5 N HCl, followed by Sr and Nd separation in cation exchange columns. Analytical conditions during the analyses on the mass spectrometer were similar to those used for the whole-rock samples. The Sr content of anhydrite, barite, and calcite samples was determined by atomic absorption with an analytical precision of ±5%, using a GBS 905AA spectrophotometer at the Atomic Absorption Laboratory of ISTO-CNRS, Orléans, France.

U–Pb dating of magmatic zircons and hydrothermal rutiles was performed at ETH—Zurich, Switzerland. High-precision "conventional" U–Pb zircon analyses were carried out on single zircon grains (except for three analyses, for which a multigrain technique was used). Selected zircons were air-abraded to remove marginal zones with lead loss, washed in warm 4 N HNO_3 and rinsed several times with distilled water and acetone in an ultrasonic bath. Dissolution and chemical extraction of U and Pb was performed using miniaturized bombs and anion exchange columns. Blanks for the entire procedure were <2 pg Pb and 0.5 pg U. A mixed $^{205}Pb/^{235}U$ tracer solution was used for all analyses. Both Pb and U were loaded with 1 μl of silica gel–phosphoric acid mixture on outgassed single Re-filaments and measured on a MAT Finnigan 262 thermal ionization mass spectrometer using an ion counter system. The performance of the ion counter system was checked by repeated measurements of the NBS 982 standard solution. The reproducibility of the $^{207}Pb/^{206}Pb$ ratio (0.467070) was better than 0.05%. The calculations of the U/Pb ratios include uncertainties of the spike calibration; Pb blank measurements, common Pb correction, U and Pb fractionation, and U decay constant errors. All uncertainties are included in the error propagation for each individual analysis. Mean age values are given at the 2σ level.

Hf isotope ratios of zircons were measured on a Nu Instruments multiple collector ICP-MS at ETH—Zurich. During analysis, the $^{176}Hf/^{177}Hf$ ratio of the JMC 475 standard was measured at 0.282141 ± 5 (1σ) using the $^{179}Hf/^{177}Hf=0.7325$ ratio for normalization (exponential law for mass correction). For the calculation of the ε-Hf values, the following present-day ratios $(^{176}Hf/^{177}Hf)_{CH}=0.28286$ and $(^{176}Lu/^{177}Hf)_{CH}=0.0334$ were used, and for 85 Ma, an average $^{176}Lu/^{177}Hf$ ratio of 0.005 for all zircons was taken into account.

Appendix 2

Table 8 Major- and trace-element analyses of whole rock samples from the southern part of the Panagyurishte district

Sample	E 59/99	E 60/99	E 17/00	E 18/00	E 19a/00	E 19/00	E 20/00	R 01/00	E 53/99A
Rock type	Muscovite gneiss	Two-mica gneiss	Variscan granite	Variscan granite	Turonian sandstone	Turonian marl	Andesite	Andesite	Andesite
SiO_2 (%)	76.78	70.77	78.80	74.79	39.67	19.38	52.16	55.19	50.51
TiO_2	0.05	0.56	0.08	0.10	0.44	0.24	0.76	0.65	0.77
Al_2O_3	15.01	14.06	12.70	14.46	9.34	5.84	18.49	15.47	16.95
Fe_2O_3	0.96	4.56	0.50	1.31	4.03	5.35	7.95	7.89	8.47
MnO	0.01	0.13	0.01	0.01	0.08	0.16	0.14	0.12	0.29
MgO	0.58	0.89	0.09	0.19	1.02	1.11	3.11	4.18	6.06
CaO	0.22	1.72	1.95	1.15	23.42	36.56	7.87	5.98	5.20
Na_2O	0.05	2.51	4.31	3.83	0.53	0.09	5.55	2.16	5.12
K_2O	4.62	1.80	0.54	3.55	1.46	0.75	0.16	4.38	0.68
P_2O_5	0.15	0.41	0.09	0.09	0.08	0.19	0.21	0.19	0.19
LOI	1.91	2.85	1.27	0.60	15.80	24.28	3.56	4.09	5.89
Total	100.33	100.25	100.34	100.08	95.88	93.92	99.97	100.32	100.13
Be (ppm)	3.6	2.1	3.0	3.2	2.3	2.3	1.4	1.1	1.9
Sc	5.4	10.7	2.3	2.6	9.6	4.6	21	26	32
V	31	56	36	31	65	58	254	240	243
Cr	10.1	22	9.3	11	41	25	18	44	30
Co	1.0	3.9	0.60	1.0	5.6	2.3	17	20	28
Ni	4.2	11	9.6	6.2	25	12	9.4	13	16
Cu	9.2	25	8.9	7.2	23	18	72	63	11
Rb	144	49	16	121	53	34	6	65	22
Sr	8.7	126	717	169	834	1139	550	503	159
Y	9.4	134	9.9	11	25	14	19	16	15
Zr	30	336	59	53	160	38	108	86	48
Nb	7.4	9.4	5.0	7.7	6.6	3.8	4.8	3.4	1.7
Cs	1.8	0.44	0.34	0.92	1.8	1.9	0.07	0.51	0.19
Ba	515	506	258	479	317	213	25	556	103
La	4.0	72	22	17	31	14	22	20	15
Ce	7.3	143	40	30	57	25	44	39	32
Pr	0.89	18	4.4	3.3	6.4	2.8	5.2	4.6	4.0
Nd	3.4	78	16	12	26	11	22	20	17
Sm	0.92	18	3.0	2.3	5.0	2.3	4.4	4.0	3.8
Eu	0.18	3.1	0.53	0.44	0.72	0.86	1.2	0.98	1.0
Gd	1.0	19	2.3	1.9	3.9	2.0	3.9	3.3	3.3
Tb	0.27	3.3	0.40	0.33	0.69	0.36	0.57	0.50	0.50
Dy	1.8	21	2.0	1.8	3.8	1.9	3.5	2.8	2.7
Ho	0.28	4.4	0.39	0.37	0.86	0.43	0.74	0.59	0.58
Er	0.86	12	0.76	1.1	2.3	1.0	1.8	1.6	1.5
Tm	0.13	1.7	0.15	0.18	0.30	0.15	0.28	0.23	0.23
Yb	1.2	12	0.91	1.2	2.3	1.1	2.1	1.8	1.7
Lu	0.22	1.7	0.15	0.16	0.30	0.14	0.31	0.23	0.23
Hf	1.3	8.5	1.9	1.7	4.0	1.2	2.8	2.3	1.4
Ta	0.96	0.24	0.66	0.68	0.38	0.30	0.32	0.19	0.07
Pb	1.6	125	5.6	12	14	10.7	10.3	10.7	2.3
Th	1.6	21	6.1	6.8	7.8	4.6	6.5	6.7	3.0
U	1.2	3.6	2.0	1.8	1.6	1.3	1.6	1.7	1.0

E 53/99B Rhyodacite	R 17/99 Rhyodacite	VV 35/99 Rhyodacite	R 19/99 Rhyodacite	VV 36/99 Subvolcanic rhyodacite	E 52/99 Subvolcanic rhyodacite	E 66/99 Subvolcanic rhyodacite	AVQ032 Subvolcanic rhyodacite	E 16/97 Elshitsa granite
72.75	69.88	70.91	71.55	71.63	70.59	69.71	69.68	72.48
0.22	0.20	0.25	0.24	0.27	0.31	0.28	0.27	0.22
13.77	14.09	15.36	14.67	14.54	14.72	14.69	17.59	14.64
2.06	2.09	2.28	2.39	2.12	2.83	3.35	2.32	2.00
0.09	0.03	0.15	0.04	0.05	0.08	0.06	0.06	0.06
1.06	2.05	0.71	1.23	0.88	1.99	2.05	2.44	0.58
1.37	0.26	1.58	2.21	1.61	0.79	0.31	0.37	2.55
3.91	2.83	4.52	4.27	4.48	4.47	3.01	2.91	3.65
2.96	4.45	3.59	0.70	2.80	2.91	4.08	4.01	3.39
0.06	0.07	0.07	0.09	0.08	0.10	0.11	0.08	0.06
2.21	2.94	0.97	2.65	1.05	1.57	2.65	n.a.	0.41
100.47	98.89	100.38	100.04	99.51	100.35	100.30	99.73	100.04
5.7	2.0	3.4	4.1	5.1	2.1	2.4	n.a.	2.0
5.2	3.0	3.8	4.6	4.7	5.9	5.0	5.5	3.6
65	62	59	62	59	72	71	n.a.	56
14	9.5	11	7.85	12	9.89	11	25	16
3.9	3.3	3.1	3.5	5.2	4.1	4.8	4.4	2.9
118	4.8	3.9	<4,1	4.8	3.5	7.7	6.1	4.5
52	13	24	5.0	9.7	16	776	1064	10
73	81	67	16	64	59	61	60	100
241	80	408	438	238	130	100	95	248
8.4	7.1	11	7.7	10	10	8.5	9.3	8.4
90	76	81	84	90	99	83	90	89
3.6	3.4	3.8	4.0	3.9	3.8	3.0	3.0	3.6
0.53	0.36	0.35	0.16	0.39	0.21	0.42	0.52	0.96
1006	500	1236	300	946	759	655	518	563
22	23	24	32	26	21	18	20	22
34	36	37	54	44	37	30	32	34
3.2	3.3	3.8	4.6	4.3	3.7	3.2	3.4	3.1
11	11	13	15	15	13	12	12	11
1.9	1.7	2.2	2.2	2.5	2.2	1.9	2.3	1.7
0.47	0.45	0.65	0.71	0.57	0.62	0.57	0.71	0.50
1.6	1.2	1.9	1.7	1.8	1.7	1.6	1.6	1.4
0.23	0.19	0.27	0.22	0.25	0.28	0.24	0.23	0.21
1.3	1.1	1.7	1.3	1.7	1.6	1.4	1.5	1.2
0.25	0.24	0.33	0.24	0.36	0.37	0.30	0.35	0.27
0.76	0.71	0.98	0.79	1.11	1.11	0.84	1.01	0.80
0.13	0.12	0.17	0.10	0.17	0.17	0.15	0.16	0.15
0.92	0.96	1.2	1.1	1.3	1.3	1.1	1.3	1.0
0.17	0.15	0.22	0.17	0.20	0.21	0.17	0.19	0.18
2.3	2.0	2.3	2.5	2.4	2.6	2.2	2.2	2.3
0.29	0.29	0.31	0.30	0.33	0.33	0.23	0.23	0.30
11.7	7.2	4.3	2.9	3.5	3.8	11.9	20.6	6.4
10.8	11	11	10	12	9.9	7.7	8.1	11
1.9	2.1	2.6	2.3	1.6	2.3	2.0	2.7	2.7

Table 8 (continued)

E 17/94 Elshitsa granite	AvQ 029 Elshitsa granite	VV 06/99 Vlaykov Vruh granodiorite	VV 23/99 Vlaykov Vruh granodiorite	AVQ 031 Vlaykov Vruh granodiorite	R 16/99 Red marl	R 15/99 Senonian flysch (marl)
73.17	70.30	70.84	69.81	70.40	17.94	12.43
0.21	0.24	0.30	0.30	0.25	0.12	0.11
14.32	13.80	15.11	15.31	17.11	2.92	2.77
2.03	2.69	3.10	3.05	1.84	1.46	1.19
0.05	0.14	0.04	0.06	0.06	0.14	0.20
0.52	0.69	1.08	1.12	0.87	0.52	0.60
2.37	2.85	1.83	2.27	2.77	43.83	45.79
3.29	3.39	3.65	4.17	3.33	0.04	0.06
3.72	3.13	2.99	2.04	3.10	0.61	0.49
0.06	0.08	0.10	0.10	0.07	0.06	0.08
0.65	n.a.	1.22	1.47	n.a.	22.61	27.82
100.38	97.31	100.26	99.69	99.80	90.27	91.54
2.0	n.a.	1.8	3.0	n.a.	<2.3	2.7
3.1	5.8	5.6	5.6	6.5	3.0	3.2
51	n.a.	78	78	n.a.	25	26
11	39	15	11	30	20	19
3.0	5.6	3.5	3.3	4.9	3.3	2.2
6.1	9.8	6.3	3.7	4.2	13	12
353	28	233	63	50	26	22
113	106	44	31	54	22	18
228	286	260	359	374	401	436
8.4	12	10	10	11	11	7.9
81	102	85	92	83	18	15
3.7	4.5	3.5	4.0	4.7	1.5	1.3
1.1	1.8	0.76	0.23	0.50	0.89	0.84
548	550	729	703	752	239	121
22	27	19	25	26	13	9.1
35	45	31	42	44	17	13
3.5	4.4	3.1	4.0	4.5	2.3	1.6
11	16	12	15	16	9.2	6.7
2.0	2.7	2.0	2.3	2.4	1.8	1.3
0.53	0.65	0.61	0.64	0.78	0.39	0.27
1.4	2.1	1.9	2.0	2.0	1.8	1.2
0.23	0.30	0.29	0.28	0.34	0.28	0.20
1.3	1.8	1.5	1.6	1.8	1.4	1.1
0.33	0.38	0.36	0.34	0.37	0.35	0.23
0.86	1.1	0.88	1.0	1.3	0.84	0.59
0.16	0.23	0.15	0.17	0.21	0.13	0.08
1.0	1.8	1.2	1.3	1.6	0.81	0.56
0.20	0.24	0.17	0.20	0.25	0.12	0.08
2.2	2.5	2.3	2.5	2.2	0.47	0.38
0.34	0.35	0.30	0.34	0.37	0.09	0.08
7.2	8.6	4.4	4.2	25.08	12.39	5.1
11	12	10	11	11	2.2	1.6
3.2	2.4	1.3	1.7	2.9	0.31	0.27

References

Aiello E, Bartolini C, Boccaletti M, Gocev P, Karagjuleva J, Kostadinov V, Manetti P (1977) Sedimentary features of the Srednogorie zone (Bulgaria): an Upper Cretaceous intra-arc basin. Sed Geol 19:39–68

Amov BG, Baldjieva TT, Arnaoudov VS, Pavlova MD (1973) Isotopic composition of lead in potassium feldspars and the geological age of pegmatites in southern Bulgaria. Comptes rendus de l'Académie bulgare des Sciences 26:1513–1516

Amov B, Bogdanov B, Baldjieva T (1974) Lead isotope composition and some features concerning the genesis and the age of the ore deposits in south Bulgaria. In: 4th IAGOD Symposium, Varna, Bulgaria, pp 13-25 (in Russian)

Amov BG, Arnaudov VS, Pavlova MA (1982) Lead isotope data and age of granitoids and metamorphic rocks from Sredna Gora and Pirin. Comptes rendus de l'Académie bulgare des Sciences 35:1535–1537

Arribas Jr. A (1995) Characteristics of high-sulfidation epithermal deposits, and their relation to magmatic fluid. In: Thompson JFH (ed) Magmas, Fluids, and Ore Deposits. Mineralogical Association of Canada, Victoria, British Columbia, pp 419–454

Arribas A, Hedenquist JW, Itaya T, Okada T, Concepcion RA, Garcia JS (1995) Contemporaneous formation of adjacent porphyry and epithermal Cu–Au deposits over 300 Ka in Northern Luzon, Philippines. Geology 23:337–340

Baumgartner R, Fontboté L, Vennemann T (2008) Mineral zoning and geochemistry of epithermal polymetallic Zn–Pb–Ag–Cu–Bi mineralization at Cerro de Pasco, Peru. Econ Geol 103:493–537

Bendezú R (2007) Shallow polymetallic and precious metal mineralization associated with a Miocene diatreme-dome complex: the Colquijirca district in the Peruvian Andes. Ph.D. thesis. University of Geneva, Terre et Environnement 64, p 221

Berza T, Constantinescu E, Vlad S-N (1998) Upper Cretaceous magmatic series and associated mineralisation in the Carpathian–Balkan region. Resour Geol 48:291–306

Boccaletti M, Manetti P, Peccerillo A (1974) The Balkanides as an instance of back-arc thrust belt: possible relations with the Hellenides. Geol Soc Am Bull 85:1077–1084

Boccaletti M, Manetti P, Peccerillo A, Stanisheva-Vassileva G (1978) Late Cretaceous high-potassium volcanism in eastern Srednogorie, Bulgaria. Geol Soc Am Bull 89:439–447

Bogdanov B (1980) Massive sulphide and porphyry copper deposits in the Panagjurishte district, Bulgaria. In: Jankovic S, Sillitoe Richard H (eds) European copper deposits; Proceedings of an international symposium. Springer-Verlag, Berlin-Heidelberg-New York, pp 50–58

Bogdanov B (1984) Hydrothermal systems of massive sulphide, porphyry-copper and vein copper deposits of Sredna Gora zone in Bulgaria. Proceedings VI Symposium IAGOD. Stuttgart, Germany, pp 63-67

Bogdanov B, Bogdanova R (1974a) The Radka copper-pyrite deposit In: Dragov P, Kolkovski B (eds) Twelve ore deposits of Bulgaria. IV symposium IAGOD, Varna, 1974, pp 114-133

Bogdanov B, Bogdanova R (1974b) Mineral parageneses in the copper-pyrite deposits from the Panagyurishte ore district (in Bulgarian). In: Alexiev E, Mincheva-Stefanova J, Radonova T (eds) Mineral genesis. Geological Institute-BAS, Sofia, pp 263–275

Bogdanov B, Bogdanova R, Chipchakova S (1970a) Intrusive ore breccias from the Radka and Elshitsa deposits in the Panagyurishte ore district. Rev Bulg Geol Soc 31:97–101 (in Bulgarian)

Bogdanov B, Popov P, Obretenov N (1970b) Structural features of the Elshitsa ore field. Rev Bulg Geol Soc 31:303–313 (in Bulgarian)

Bogdanov B, Popov P, Obretenov N (1972a) Structure of the Elshitsa copper–pyrite deposit. Annuaire de l'Ecole Supérieure des Mines et de Géologie 18:27–39 (in Bulgarian)

Bogdanov B, Ignatovski P, Popov P, Obretenov N (1972b) Structure of the Vlaykov Vruh ore deposit. Bull Geol Institute - Series Metallic and Non-metallic Mineral Deposits 21:23–36 (in Bulgarian)

Bogdanov K, Tsonev D, Kuzmanov K (1997) Mineralogy of gold in the Elshitsa massive sulphide deposit, Sredna Gora zone, Bulgaria. Miner Deposita 32:219–229

Boyadjiev S, Chipchakova S (1962) Petrology of the Elshitsa-Boshulia pluton. Ann de la Dir Gen de Géol 13:5–71 (in Bulgarian with English abstract)

Boyadjiev S, Chipchakova S (1965) The dyke formation in the Panagyurishte area. Bull Inst Sci de Rech Géol Dir Gen de Géol 2:75–110 (in Bulgarian with English abstract)

Brathwaite RL, Simpson MP, Faure K, Skinner DNB (2001) Telescoped porphyry Cu-Mo-Au mineralisation, advanced argillic alteration and quartz-sulphide-gold-anhydrite veins in the Thames District, New Zealand. Miner Deposita 36:623–640

Carrigan CW, Mukasa SB, Haydoutov I, Kolcheva K (2005) Age of Variscan magmatism from the Balkan sector of the Orogen, central Bulgaria. Lithos 82:125–147

Chambefort I, Moritz R (2006) Late Cretaceous structural control and alpine overprint of the high-sulfidation Cu–Au epithermal Chelopech deposit, Srednogorie belt, Bulgaria. Miner Deposita 41:259–280

Chambefort I, Moritz R, von Quadt A (2007) Petrology, geochemistry and U–Pb geochronology of magmatic rocks from the high-sulphidation epithermal Cu–Au Chelopech deposit, Srednogorie zone, Bulgaria. Miner Deposita 42:665–690

Cheshitev G, Milanova V, Sapounov I, Choumachenko P (1995) Teteven map sheet. Explanatory note to the Geological Map of Bulgaria in scale 1:100,000, pp 94 (in Bulgarian)

Chipchakova S, Stefanov D (1974) Genetic types of argillisites at the height of Golyamo Petelovo and in the Elshitsa–West copper–pyrite deposit in the Panagyurishte ore district. In: Alexiev E, Mincheva-Stefanova J, Radonova T (eds) Mineral genesis. Geological Institute-BAS, Sofia, pp 437–454

Ciobanu CL, Cook NJ, Stein H (2002) Regional setting and geochronology of the Late Cretaceous Banatitic Magmatic and Metallogenetic Belt. Miner Deposita 37:541–567

Claypool GE, Holster WT, Kaplan IR, Sakai H, Zak I (1980) The age curves of sulfur and oxygen isotopes in marine sulfate and their mutual interpretation. Chem Geol 28:199–260

Cooke DR, Bloom MS (1990) Epithermal and subjacent porphyry mineralization, Acupan, Baguio district, Philippines—a fluid inclusion and paragenetic study. J Geochem Explor 35:297–340

Corbett GJ, Leach TM (1998) Southwest Pacific Rim gold–copper systems: structure, alteration, and mineralization. SEG Special Publications 6:237p

Dabovski C (1963) Structural features of the Elshitsa–Boshulia pluton. Annuaire de la Direction Génerale de Géologie 14:19–46 (in Bulgarian)

Dabovski C, Zagorchev I, Rouseva M, Chounev D (1972) Paleozoic granitoides in the Sushtinska Sredna Gora. Ann UGP 16:57–92 (in Bulgarian)

Dabovski C, Harkovska A, Kamenov B, Mavrudchiev B, Stanisheva-Vassileva G, Yanev Y (1991) A geodynamic model of the Alpine magmatism in Bulgaria. Geol Balc 21:3–15

Daieva L, Chipchakova S (1997) Geochemical features of the Upper Cretaceous magmatites from the Panagyurishte volcano-intrusive region, Central Srednogorie. Geochemistry, Mineralogy and Petrology 32:85–99 (in Bulgarian with English abstract)

Dimitrov C (1960) Magmatismus und Erzbildung im Erzgebiet von Panagjuriste. Freiberg Forschungshefte C 79:67–81

Dimitrov C (1985) On the genesis of the Elshitsa, Radka, Krassen and Bialata Prast ore deposits, Panagyurishte area (in Bulgarian). Rev Bulg Geol Soc 46:257–266

Drew LJ (2005) A tectonic model for the spatial occurrence of porphyry copper and polymetallic vein deposits—applications to Central Europe USGS Scientific Investigations Report 2005-5272, pp 36

Dupont A, Vander Auwera J, Pin C, Marincea S, Berza T (2002) Trace element and isotope (Sr, Nd) geochemistry of porphyry- and skarn-mineralising Late Cretaceous intrusions from Banat, western South Carpathians, Romania. Miner Deposita 37:568–586

Einaudi MT, Hedenquist JW, Inan EE (2003) Sulfidation state of fluids in active and extinct hydrothermal systems: transitions from porphyry to epithermal environments. SEG Special Publication 10:285–313

Georgiev N, Lazarova A (2003) Magma mixing in Upper Cretaceous plutonic bodies in the southwestern parts of the Central Sredna Gora zone, Bulgaria. Comptes rendus de l'Académie bulgare des Sciences 56:47–52

Günther D, von Quadt A, Wirz R, Cousin H, Dietrich VJ (2001) Elemental analyses using laser ablation-inductively coupled plasma-mass spectrometry (LA-ICP-MS) of geological samples fused with Li2B4O7 and calibrated without matrix-matched standards. Mikrochim Acta 136:101–107

Handler R, Neubauer E, Velichkova SH, Ivanov Z (2004) 40Ar/39Ar age constraints on the timing of magmatism and postmagmatic cooling in the Panagyurishte region, Bulgaria. Schweiz Mineral Petrogr Mitt 84:119–132

Hart SR, Zindler A (1989) Constraints on the nature and development of chemical heterogeneities in the mantle. In: Peltier WR (ed) Mantle convection. Gordon and Breach Science Publishers, New York, pp 261–382

Haydoutov I (2001) The Balkan island-arc association in west Bulgaria. Geol Balc 31:109–110

Hedenquist JW, Lowenstern JB (1994) The role of magmas in the formation of hydrothermal ore-deposits. Nature 370:519–527

Hedenquist JW, Arribas A, Reynolds TJ (1998) Evolution of an intrusion-centered hydrothermal system: Far Southeast-Lepanto porphyry and epithermal Cu–Au deposits, Philippines. Econ Geol 93:373–404

Hedenquist JW, Arribas R. A, Gonzalez-Urien E (2000) Exploration for epithermal gold deposits. In: Hagemann SG, Brown PE (eds) Gold in 2000. Reviews in Econ Geol 13, pp 245–277.

Hedenquist JW, Claveria RJR, Villafuerte GP (2001) Types of sulfide-rich epithermal deposits, and their affiliation to porphyry systems: Lepanto–Victoria–Far Southeast deposits, Philippines, as examples. In: ProExplo Congreso. Lima, Peru, 24–28 April, 2001, electronic version

Heinrich CA (2005) The physical and chemical evolution of low-salinity magmatic fluids at the porphyry to epithermal transition: a thermodynamic study. Miner Deposita 39:864–889

Heinrich CA, Neubauer F (2002) Cu–Au–Pb–Zn–Agmetallogeny of the Alpine–Balkan–Carpathian–Dinaride geodynamic province. Miner Deposita 37:533–540

Ignatovski P, Bayraktarov I (1996) Panagyurishte ore district. In: Popov P (ed) Plate tectonic aspects of the Alpine metallogeny in the Carpatho-Balkan region, UNESCO-IGCP project 356, Proceedings of the annual meeting. Sofia, Bulgaria, 1996. pp 155–157

Ignatovski P et al. (1990) Metallogenic and prognostic map of the Panagyurishte ore district in scale 1:25,000.Geological report n° 028006. Geological Committee, NIPI, pp 253 (in Bulgarian)

Ivanov Z (1989a) Structure and tectonic evolution of central parts of the Rhodope massif. In: Ivanov Z (ed) Structure and Geodynamic Evolution of the inner zones of Balkanides–Kraishtides and Rhodope Area. Guide for excursion, XIV Congress CBGA, Sofia, Bulgaria. pp 56–92

Ivanov Z, (ed.) (1989b) Structure and tectonic evolution of the central parts of the Rhodope massif. Guide for excursion E-3, XIV Congress CBGA, Sofia, Bulgaria

Ivanov Z, Henry B, Dimov D, Georgiev N, Jordanova D, Jordanova N (2001) New model for Upper Cretaceous magma emplacement in the southwestern parts of Central Srednogorie - Petrostructural and AMS data. In: ABCD-GEODE 2001, Workshop, Abstracts volume. Vata Bai, Romania, pp 60–61

Ivanov Z, Georgiev N, Lazarova A, Dimov D (2002) New model of Upper Cretaceous magma emplacement in the southwestern parts of Central Sredna Gora zone—Bulgaria. In: Proceedings of the XVII Congress of Carpathian–Balkan Geological Association, Bratislava, September 1–4, 2002, electronical version

Jacquat S (2003) Etude Paragénétique et Géochimique du Gisement Epithermal d'Or et de Cuivre de type "High-Sulfidation" de Chelopech, Bulgarie. Unpublished MSc thesis. University of Geneva, pp 172

Jankovic S (1977) The copper deposits and geotectonic setting of Tethyan Eurasian metallogenic belt. Miner Deposita 12:37–47

Jannas RR, Bowers TS, Petersen U, Beane RE (1999) High-sulfidation deposit types in the El Indio district, Chile. In: Skinner BJ (ed) Geology and Ore Deposits of the Central Andes. pp 219–266

Kamenov B, Dabovski C, Harkovska A, Maneva B, Mavroudchiev B, Stanisheva-Vassileva G, Vassilev L, Yanev Y (2000) Late Cretaceous and Tertiary magmatism and related metallogeny in Bulgaria: Review and problems. In: ABCD-GEODE 2000 Workshop—Abstracts. Borovets, Bulgaria, pp 33

Kamenov BK, von Quadt A, Peytcheva I (2002) New insight into petrology, geochemistry and dating of the Vejen pluton, Bulgaria. Geochemistry, Mineralogy and Petrology 39:3–25

Kamenov B, Nedialkov R, Yanev Y, Stoykov S (2003a) Petrology of the Late Cretaceous ore-magmatic centres in the Central Srednogorie, Bulgaria. In: Bogdanov K, Strashimirov S (eds) Cretaceous porphyry–epithermal systems of the Srednogorie zone, Bulgaria. SEG Guidebook Series 36, pp 27–46.

Kamenov BK, von Quadt A, Peytcheva I (2003b) Capitan–Dimitrievo pluton in Central Srednogorie, Bulgaria: mineral chemistry, geochemistry and isotope evidence for magma-mixing origin. Geochemistry, Mineralogy and Petrology 40:21–53

Kamenov BK, Yanev Y, Nedialkov R, Moritz R, Peytcheva I, von Quadt A, Stoykov S, Zartova A (2007) Petrology of Upper Cretaceous island-arc ore-magmatic centers from the Central Srednogorie, Bulgaria: magma evolution and paths. Geochemistry, Mineralogy and Petrology (Sofia) 45:39–77

Karagjuleva J, Kostadinov V, Tzankov T, Gochev P (1974) Structure of the Panagyurishte strip east of the Topolnica river. Geol. Inst. Bull.-Geotectonics, Sofia 23:231–301 in Bulgarian

Karamata S, Knezevic V, Pecskay Z, Djordjevic M (1997) Magmatism and metallogeny of the Ridanj–Krepoljin belt (eastern Serbia) and their correlation with northern and eastern analogues. Miner Deposita 32:452–458

Kesler SE, Campbell IH, Smith CN, Hall CM, Allen CM (2005) Age of the Pueblo Viejo gold–silver deposit and its significance to models for high-sulfidation epithermal mineralization. Econ Geol 100:253–272

Koepnick RB, Burke WH, Denison RE, Hetherington EA, Nelson HF, Otto JB, Waite LE (1985) Construction of the seawater 87Sr/86Sr curve for the cenozoic and cretaceous: supporting data. Chem Geol 58:55–81

Kolkovski B, Popov P, Tsvetanov R, Naftali L, Darakchiev G, Cholakova N, Vangelov I (1977) Geological structure and prognosis evaluation of the Popovo Dere ore manifestation, Panagyurishte ore district. Geological report n° 6/1974 - Earth Sciences Center - Sofia University "St. Kliment Ohridski", pp 159(in Bulgarian)

Kouzmanov K (2001) Genèse des concentrations en métaux de base et précieux de Radka et Elshitsa (zone de Sredna Gora, Bulgarie): une approche par l'étude minéralogique, isotopique et des

inclusions fluids. Unpublished Ph.D. thesis. Université d'Orléans, p 437

Kouzmanov K, Moritz R, Chiaradia M, Fontignie D, Ramboz C (2001) Sr and Pb isotope study of Au-Cu epithermal and porphyry-Cu deposits from the southern part of the Panagyurishte district, Sredna Gora zone, Bulgaria. In: Piestrynski A et al. (eds) Mineral deposits at the beginning of the 21st century, Proceedings of the joint 6th biennial SGA-SEG meeting, Krakow, Poland, 26–29 August 2001. A.A.Balkema Publishers, pp 539–542

Kouzmanov K, Bailly L, Ramboz C, Rouer O, Bény J-M (2002) Morphology, origin and infrared microthermometry of fluid inclusions in pyrite from the Radka epithermal copper deposit, Srednogorie zone, Bulgaria. Miner Deposita 37:599–613

Kouzmanov K, Ramboz C, Lerouge C, Deloule E, Beaufort D, Bogdanov K (2003) Stable isotopic constrains on the origin of epithermal Cu-Au and related porphyry copper mineralisation in the southern Panagyurishte district, Srednogorie zone, Bulgaria. In: Elioupoulos DG et al. (eds) Mineral Expolration and Sustainable Development, Proceedings of the 7th biennial SGA meeting, Athens, Greece, 24–28 August 2003. A.A.Balkema Publishers, pp 1181–1184

Kouzmanov K, Ramboz C, Bailly L, Bogdanov K (2004) Genesis of high-sulfidation vinciennite-bearing Cu–As–Sn (+Au) assemblage from the Radka copper epithermal deposit, Bulgaria: evidence from mineralogy and infrared microthermometry of enargite. Can Mineral 42:1501–1521

Kouzmanov K, Bogdanov K, Ramboz C (2005) Te- and Bi-bearing assemblages in the Elshitsa and Radka epithermal deposits, Central Srednogorie, Bulgaria: Mineralogy and genetical features. In: Cook NJ, Bonev IK (eds) Au–Ag–Te–Se deposits, IGCP Project 486, Proceedings of the 2005 Field Workshop, Kiten, Bulgaria, 14–19 September 2005. pp 108–112

Kuno H (1968) Differentiation of basalt magmas. In: Hess HH, Poldervaart A (eds) Basalts: the Poldervaart treatise on rocks of basaltic composition. pp, New York, pp 623–688

Le Maitre RW, Bateman P, Dudek A, Keller J, Lameyre J, Le Bas MJ, Sabine PA, Schmid R, Sorensen H, Streckeisen A, Woolley AR, Zanettin B (1989) A classification of igneous rocks and glossary of terms. Blackwell Scientific Publications, Oxford, p 193

Lilov P, Chipchakova S (1999) K–Ar dating of the Upper Cretaceous magmatic rocks and hydrothermal metasomatic rocks from the Central Srednogorie. Geochemisty, Mineralogy and Petrology 36:77–91 (in Bulgarian)

Lips ALW (2002) Correlating magmatic-hydrothermal ore deposit formation over time with geodynamic processes in SE Europe. In: Blundell DJ, Neubauer F, von Quadt A (eds) The timing and location of major ore deposits in an evolving orogen, pp 69–79

McDonough WF, Sun SS (1995) The composition of the earth. Chem Geol 120:223–253

Moev M, Antonov M (1978) Stratigraphy of the Upper Cretaceous in the eastern part of the Sturguel–Chelopech strip. Ann de l'Ec Sup Min Géol 23:7–30 (in Bulgarian)

Moritz R, Chambefort I, Chiaradia M, Fontignie D, Petrunov R, Simova S, Arisanov A, Doychev P (2001) The Late Cretaceous high-sulfidation Au–Cu Chelopech deposit, Bulgaria: geological setting, paragenesis, fluid inclusion microthermometry of enargite, and isotope study (Pb, Sr, S). In: Piestrynski A et al. (eds) Mineral deposits at the beginning of the 21st century, Proceedings 6th biennial SGA meeting, Krakow, Poland. A.A.Balkema Publishers, pp 547–550

Moritz R, Jacquat S, Chambefort I, Fontignie D, Petrunov R, Georgieva S, von Quadt A (2003) Controls of ore formation at the high-sulphidation Au–Cu Chelopech deposit, Bulgaria: evidence from infrared fluid inclusion microthermometry of enargite and isotope systematics of barite. In: Elioupoulos DG et al (eds) Mineral exploration and sustainable development, Proceedings 7th biennial SGA meeting, Athens, Greece, 24–28 August 2003. Millpress, Rotterdam, pp 1209–1212

Moritz R, Kouzmanov K, Petrunov R (2004) Late Cretaceous Cu–Au epithermal deposits of the Panagyurishte district, Srednogorie zone, Bulgaria. Schweiz Mineral Petrogr Mitt 84:79–99

Müller D, Kaminski K, Uhlig S, Graupner T, Herzig PM, Hunt S (2002) The transition from porphyry- to epithermal-style gold mineralization at Ladolam, Lihir Island, Papua New Guinea: a reconnaissance study. Miner Deposita 37:61–74

Muntean JL, Einaudi MT (2000) Porphyry gold deposits of the Refugio district, Maricunga belt, northern Chile. Econ Geol 95:1445–1472

Muntean JL, Einaudi MT (2001) Porphyry–epithermal transition: Maricunga belt, northern Chile. Econ Geol 96:743–772

Mutafchiev I, Petrunov R (1996) Geological genetic models of ore-deposit formation in the Panagyurishte–Etropole ore region. Unpublished report for Chelopech LTD, Sofia, pp 69

Nachev I, Nachev C (1986) Sedimentology of the Upper Cretaceous in the Panagyurishte district. I. Results of the studies. Palaentology, Stratigraphy & Lithology, Sofia 22:35–70 in Bulgarian

Neubauer F (2002) Contrasting Late Cretaceous with Neogene ore provinces in the Alpine–Balkan–Carpathian–Dinaride collision belt. In: Blundell DJ, Neubauer F, von Quadt A (eds) The Timing and Location of Major Ore Deposits in an Evolving Orogen, pp 81–102

Peycheva I, von Quadt A (2004) The Palaeozoic protoliths of Central Srednogorie, Bulgaria: records in zircons from basement rocks and Cretaceous migmatites. In: 5th International Symposium on Eastern Mediterranean Geology, Thessaloniki, Greece, 14–20 April, Ref:T11-9.

Peytcheva I, von Quadt A, Kouzmanov K, Bogdanov K (2003) Elshitsa and Vlaykov Vruh epithermal and porphyry Cu (Au) deposits of Central Srednogorie, Bulgaria: source and timing of magmatism and mineralisation. In: Elioupoulos DG et al. (eds) Mineral Expolration and Sustainable Development, Proceedings of the 7th biennial SGA meeting, Athens, Greece, 24–28 August 2003. A.A.Balkema Publishers, pp 371–373

Peytcheva I, von Quadt A, Georgiev N, Ivanov Z, Heinrich CA, Frank M (2008) Combining trace-element compositions, U–Pb geochronology and Hf isotopes in zircons to unravel complex calcalkaline magma chambers in the Upper Cretaceous Srednogorie zone (Bulgaria). Lithos 104:405–427

Popov K (2001) Geology of the southern part of Panagyurishte ore region. Annual of the University of Mining and Geology, Sofia 43–44:51–63

Popov K (2005) Lithostratigraphy of the Late Cretaceous rocks in the Panagyurishte ore region. Annual of the University of Mining and Geology "St. Ivan Rilski" 48, Part I, Geology and Geophysics: 101–114

Popov P, Popov K (1997) Metallogeny of Panagyurishte ore region. In: Romic K, Kondzulovic R (eds) Symposium "Ore Deposits Exploration", 2–4 April 1997. Belgrade, pp 327–338

Popov P, Popov K (2000) General geologic and metallogenic features of the Panagyurishte ore region. In: Strashimirov S, Popov P (eds) Geology and metallogeny of the Panagyurishte ore region (Srednogorie zone, Bulgaria), ABCD-GEODE 2000 workshop, Borovets, Bulgaria. Guidebook to excursions (A and C). Publishing House "St Ivan Rilski", Sofia, pp 1–7

Popov P, Tsonev D, Kanazirski M (2000) Elshitsa ore field. In: Strashimirov S, Popov P (eds) Geology and metallogeny of the Panagyurishte ore region (Srednogorie zone, Bulgaria), ABCD-GEODE 2000 workshop, Borovets, Bulgaria, Guidebook to excursions (A and C). Publishing House "St. Ivan Rilski", Sofia, pp 40–46

Popov P, Berza T, Grubic A, Ioane D (2002) Late Cretaceous Apuseni–Banat–Timok–Srednogorie (ABTS) magmatic and met-

allogenic belt in the Carpathian–Balkan orogen. Geologica Balcanica 32:145–163

Popov P, Strashimirov S, Popov K, Petrunov R, Kanazirski M, Tzonev D (2003) Main features in geology and metallogeny of the Panagyurishte ore region. 50 years University of Mining and Geology "St. Ivan Rilski" Annual 46, part I, Geology and Geophysics, Sofia: 119–125

Radonova T (1967a) Dumortierite from the area of the Elshitsa ore deposit. Panagyurishte district Rev Bulg Geol Soc 28:191–195 (in Bulgarian)

Radonova T (1967b) Hydrothermally altered zone in the area of the Elshitsa mine, Panagyurishte district. Bull Geol Institute-Ser Geochemistry, Mineralogy and Petrology 17:189–204 in Bulgarian

Radonova T (1970) Certain petrogenetic factors controlling copper pyrite mineralizations in the Central Srednogorie. Rev Bulg Geol Soc 31:323–328 (in Bulgarian)

Saunders AD, Tarney J, Weaver SD (1980) Transverse geochemical variations across the Antarctic Peninsula—implications for the genesis of calc-alkaline magmas. Earth Planet Sci Lett 46:344–360

Seedorff E, Dilles JH, Proffett JMJ, Einaudi MT, Zurcher L, Stavast WJA, Johnson DA, Barton MD (2005) Porphyry deposits: characteristics and origin of hypogene features. Econ Geol 100th Anniversary Volume: 251–298

Sillitoe RH, Hedenquist JW (2003) Linkages between volcanotectonic settings, ore-fluid compositions, and epithermal precious metal deposits. SEG Special Publication 10:315–343

Stanisheva-Vassileva G (1980) The Upper Cretaceous magmatism in Srednogorie zone, Bulgaria: a classification attempt and some implications. Geol Balc 10:15–36

Stoykov S, Yanev Y, Moritz R, Fontignie D (2003) Petrology, Sr and Nd isotope signature of the Late Cretaceous magmatism in the south-eastern part of the Etropole Stara Planina, Srednogorie magmatic zone. 50 years University of Mining and Geology "St. Ivan Rilski". Ann Volume 46:161–167

Stoykov S, Peytcheva I, von Quadt A, Moritz R, Frank M, Fontignie D (2004) Timing and magma evolution of the Chelopech volcanic complex (Bulgaria). Schweiz Mineral Petrogr Mitt 84:101–117

Strashimirov S, Kovachev V (1992) Temperatures of ore-formation in copper deposits from the Srednogorie zone based on fluid inclusion studies of minerals. Rev Bulg Geol Soc 53:1–12 (in Bulgarian)

Strashimirov S, Petrunov R, Kanazirski M (2002) Porphyry–copper mineralisation in the central Srednogorie zone, Bulgaria. Miner Deposita 37:587–598

Strashimirov S, Bogdanov K, Popov K, Kehayov R (2003) Porphyry systems of the Panagyurishte ore region. In: Bogdanov K, Strashimirov S (eds) Cretaceous porphyry–epithermal systems of the Srednogorie zone, Bulgaria. SEG Guidebook Series 36, pp 47–78

Sun SS, McDonough WF (1989) Chemical and isotopic systematics of oceanic basalts: implications for mantle composition and processes. In: Saunders AD, Norry MJ (eds) Magmatism in ocean basins. Geol. Soc. London Spec. Pub., pp 313–345

Tarkian M, Hünken U, Tokmakchieva M, Bogdanov K (2003) Precious-metal distribution and fluid-inclusion petrography of the Elatsite porphyry copper deposit, Bulgaria. Miner Deposita 38:261–281

Taylor HP Jr (1974) The application of oxygen and hydrogen isotope studies to problems of hydrothermal alteration and ore deposition. Econ Geol 69:843–883

Tsonev D, Popov K, Kanazirski M, Strashimirov S (2000) Radka ore field. In: Strashimirov S, Popov P (eds) Geology and metallogeny of the Panagyurishte ore region (Srednogorie zone, Bulgaria), ABCD-GEODE 2000 Workshop, Guide to excursions (A and C). pp 32–39

Vassilev P, Fargova V (1998) The Petelovo gold deposit. Geology and Mineral Resources 1:22–23

von Quadt A, Peytcheva I, Kamenov B, Fanger L, Heinrich CA, Frank M (2002) The Elatsite porphyry copper deposit in the Panagyurishte ore district, Srednogorie zone, Bulgaria: U–Pb zircon geochronology and isotope-geochemical investigations of magmatism and ore genesis. In: Blundell DJ, Neubauer F, von Quadt A (eds) The Timing and Location of Major Ore Deposits in an Evolving Orogen., pp 119–135

von Quadt A, Peycheva I, Cvetkovic V (2003) Geochronology, geochemistry and isotope tracing of the Cretaceous magmatism of East-Serbia and Panagyurishte district (Bulgaria) as part of the Apuseni–Timok–Srednogorie metallogenic belt in Eastern Europe. In: Elioupoulos DG et al. (eds) Mineral Exploration and Sustainable Development, Proceedings of the 7th biennial SGA meeting, Athens, Greece, 24–28 August 2003. A.A. Balkema Publishers, pp 407–410

von Quadt A, Moritz R, Peytcheva I, Heinrich CA (2005) Geochronology and geodynamics of Late Cretaceous magmatism and Cu–Au mineralization in the Panagyurishte region of the Apuseni–Banat–Timok–Srednogorie belt, Bulgaria. Ore Geol Rev 27:95–126

Yossifov D, Pčelarov V (1977) A scheme of the thickness of the Earth's crust in the Balkan peninsula and some features of its structure). Geol Balc 7:7–22 (in Russian with English abstract)

Zartman RE, Doe BR (1981) Plumbotectonics—the model. Tectonophysics 75:135–162

Zindler A, Hart S (1986) Chemical geodynamics. Annu Rev Earth Planet Sci 14:493–571